Electromagnetic effects in light nuclei and the cluster potential model

S. B. Dubovichenko and A. V. Dzhazairov-Kakhramanov
Kazakh State National University, Alma-Ala

Fiz. Élem. Chastits At. Yadra **28**, 1529–1594 (November–December 1997)

Photodisintegration and radiative capture in the N^2H, N^3H, N^3He, $^2H^2H$, $^2H^3He$, $^2H^4He$, $^3He^3H$, $^4He^3H$, and $^4He^3He$ channels are studied on the basis of the corresponding two-cluster potential models. The astrophysical S factors at low energies are calculated. It is shown that various electromagnetic characteristics of light nuclei, including the Coulomb form factors at momenta of up to 4 F^{-1}, can be studied using a single set of intercluster interactions containing forbidden states and consistent with the phase shifts of the cluster low-energy elastic scattering. The calculated inelastic form factors have a second maximum at 3–4 F^{-1}, although it is lower than the experimental one. The orbital states are classified for the lightest cluster systems, and the phase shifts and intercluster potentials are separated on the basis of Young orbital schemes. © *1997 American Institute of Physics.* [S1063-7796(97)00406-3]

1. INTRODUCTION

Over two decades ago, in Refs. 1 and 2 it was shown for the first time that the phase shifts of the elastic scattering of light cluster systems can be described using deep, purely attractive potentials of the Woods–Saxon type containing forbidden bound states. The structure of a forbidden state is determined by the permutational symmetry of the wave functions of the system under nucleon permutations. The phase shifts at zero energy for a given type of interaction obey a generalized Levinson theorem:[2]

$$\delta_L = \pi(N_L + M_L),$$

where N_L and M_L are the numbers of forbidden and allowed bound states. The phase shifts at high energies tend to zero, while always remaining positive. This approach can apparently be viewed as an alternative to the repulsive core, which is introduced to qualitatively take into account the Pauli principle without completely antisymmetrizing the wave function. The radial wave function of the allowed states of potentials containing forbidden states oscillates at small distances, but does not die out, as in the case of interactions with a core.

Later on, Gaussian potentials containing forbidden states were obtained[3] which have parameters consistent with the elastic-scattering phase shifts. It was shown that the use of these potentials in simple one-channel $^4He^3H$ and $^4He^2H$ cluster models allows a quite successful description of several characteristics of the ground states of the ^6Li and ^7Li nuclei, the probability of clusterization of which in these channels is relatively high. Various estimates give 0.6–0.8 for the $^4He^2H$ clusterization and about 0.9 for the $^4He^3H$ system.[4] The success of the one-channel model based on these potentials is due not only to the high degree of clusterization of these nuclei, but also to the fact that in each state of the clusters there is only one allowed orbital Young scheme[2,5] determining the symmetry of this state. A sort of "unified" description of the continuous and discrete spectra is thereby obtained, and the potentials found from the experimental phase shifts can be used quite successfully for describing various characteristics of the ground states of lithium nuclei. The cluster potential model is used in these calculations. It is assumed that the nucleus consists of two structureless fragments which can be associated with the properties of the corresponding particles in the free state. The wave function of the system is not antisymmetrized, but the intercluster interactions contain forbidden states.[3]

For lighter cluster systems like N^2H, $^2H^2H$, N^3H, N^3He, and $^2H^3He$, mixing of orbital symmetries is already possible in scattering states with the minimum spin, and the situation becomes more complicated. Two orbital symmetries with different Young schemes are allowed in continuum states with the minimum spin, while only a single scheme apparently corresponds to the bound ground state.[6–8] Therefore, the potentials obtained directly from the experimental phase shifts effectively depend on different orbital schemes and cannot be used in that form for describing the ground-state characteristics. It is necessary to extract from these interactions the pure component used to analyze the bound-state characteristics. The results then will mainly depend on the degree of clusterization of the nucleus in the channels in question.

It was shown in Refs. 6–8 that for the lightest cluster systems the experimental mixed phase shifts can be represented as half the sum of the pure phase shifts with definite Young schemes. It is usually assumed that one of the pure phase shifts of the channel with the minimum spin can be taken to be the analogous pure phase shift of another spin state or system which is pure in isospin. In this case from the experimental phase shifts it is easy to find the pure phase shift of maximum symmetry of the channel with the minimum spin and use it to parametrize pure interactions. In particular, the N^2H, N^3H, N^3He, $^2H^2H$, and $^2H^3He$ pure Gaussian interactions were obtained in Refs. 6–8, and it was shown[8] that on the whole it is possible to correctly reproduce the binding energy of the ^3H, ^3He, and ^4He nuclei in cluster channels, the asymptotic constant, the charge radius, and the elastic Coulomb form factor at small momentum transfers.

It should be noted that mixing in the orbital Young schemes in states with the minimum spin is characteristic not only of the majority of light cluster systems, but is also re-

alized in heavier systems of the form N^6Li, N^7Li, and $^2H^6Li$ (Ref. 9).

The interactions obtained earlier have also been used to study the cross sections for photoprocesses with the same cluster models, which despite their simplicity allow good results to be obtained in some cases using potentials whose parameters are initially fixed from the experimental phase shifts and practically do not change in the later calculations.[6,7,10]

1. THE COMPUTATIONAL METHODS

The following well known expression[11] is used to calculate the cross sections of photoprocesses in the long-wavelength approximation:

$$\frac{d\sigma_c(N)}{d\Omega}=\frac{K\mu}{2\pi\hbar^2 q}\frac{1}{(2S_1+1)(2S_2+1)}\times\sum_{m_1\cdot m_1,\lambda}|M_{J\lambda}(N)|^2, \tag{1}$$

where $N=E$ or M, and

$$M_{J\lambda}(N)=\sum_J i^J\sqrt{2\pi(2J+1)}\,\frac{K^J}{(2J+1)!!}\left[\frac{J+1}{J}\right]^{1/2}\lambda\times\sum_m D^J_{m\lambda}\langle f|H_{Jm}(N)|i\rangle,$$

$$H_{Jm}(E)=Q_{Jm}(L)+Q_{Jm}(S),$$

$$H_{Jm}(M)=W_{Jm}(L)+W_{Jm}(S),$$

$$Q_{Jm}(L)=e\sum_i Z_i r_i^J Y_{Jm}(Q_i),$$

$$Q_{Jm}(S)=-\frac{e\hbar}{m_0c}K\left[\frac{J}{J+1}\right]^{1/2}\sum_i \mu_i\hat{S}_i r_i^J Y_{Jm}(\Omega_i),$$

$$W_{Jm}(L)=i\frac{e\hbar}{m_0c}\frac{1}{J+1}\sum_i\frac{Z_i}{M_i}\hat{L}_i\nabla_i(r_i^J Y_{Jm}(\Omega_i)),$$

$$W_{Jm}(S)=i\frac{e\hbar}{m_0c}\sum_i\mu_i\hat{S}_i\nabla_i(r_i^J Y_{Jm}(\Omega_i)).$$

Here J is the multipole order; q is the wave number of the relative motion of the clusters; $D^J_{m\lambda}$ is the Wigner function; μ is the reduced mass; M_i, Z_i, $\hat{S}_i$, and $\hat{L}_i$ are the masses, charges, spins, and orbital angular momenta of the clusters; μ_i are the cluster magnetic moments; K is the photon wave number; and m_0 is the nucleon mass. The sign of the operator $Q_{Jm}(S)$ is chosen to be negative, as in Ref. 12. Integrating over angles and summing over λ, for the total capture cross section we obtain[10]

$$\sigma_c(J)=\frac{8\pi K^{2J+1}}{\hbar^2 q}\frac{\mu}{(2S_1+1)(2S_2+1)}\frac{J+1}{J[(2J+1)!!]^2}\times\sum_{m,m_i,m_f}|M_{Jm}(N)|^2,$$

$$M_{Jm}(N)=i^J\langle f|H_{Jm}(N)|i\rangle, \tag{2}$$

where in the cluster model the electromagnetic operators take the form

$$Q_{Jm}(L)=e\mu^J\left[\frac{Z_1}{M_i^J}+(-1)^J\frac{Z_2}{M_2^J}\right]R^J Y_{Jm}=A_J R^J Y_{Jm},$$

$$Q_{Jm}(S)=-\frac{e\hbar}{m_0c}K\left[\frac{J}{J+1}\right]^{1/2}\left[\mu_1\hat{S}_1\frac{M_2^1}{M^J}+(-1)^J\mu_2\hat{S}_2\frac{M_1^J}{M^J}\right]R^J Y_{Jm}$$

$$=(B_{1J}\hat{S}_{1J}+B_{2J}\hat{S}_2)R^J Y_{Jm},$$

$$W_{Jm}(L)=i\frac{e\hbar}{m_0c}\frac{\sqrt{J(2J+1)}}{J+1}\left[\frac{Z_1}{M_1}\frac{M_2^J}{M^J}+(-1)^{J-1}\frac{Z_2}{M_2}\frac{M_1^J}{M^J}\right]R^{J-1}\hat{L}Y^{J-1}_{Jm}$$

$$=C_J R^{J-1}\hat{L}Y^{J-1}_{Jm},$$

$$W_{Jm}(S)=i\frac{e\hbar}{m_0c}\sqrt{J(2J+1)}\left[\mu_1\hat{S}_1\frac{M_2^{J-1}}{M^{J-1}}+(-1)^{J-1}\mu_2\hat{S}_2\frac{M_1^{J-1}}{M^{J-1}}\right]R^{J-1}Y^{J-1}_{Jm}$$

$$=(D_{1J}\hat{S}_1+D_{21}\hat{S}_2)R^{J-1}.$$

Here R is the intercluster separation, and M is the nuclear mass. In what follows we shall use the cluster bound-state wave functions in the usual form[3]

$$|f\rangle=\Psi_f=\sum_{L_f J_f}R_{L_f J_f}\Phi^{L_f S}_{J_f m_f},\quad R_{LJ}=\frac{U_{LJ}}{r}. \tag{3}$$

We write the scattering function as[11]

$$|i\rangle=\Psi_i=\frac{1}{q}\sum_{L_i J_i}i^{L_i}\sqrt{4\pi(2L_i+1)}\times(L_i 0 S m_i|J_i m_i)e^{i\delta_{L_i J_i}}R_{L_i J_i}\Phi^{L_i S}_{J_i m_i}. \tag{4}$$

Here R_{LJ} is the radial wave function obtained by solving the Schrödinger equation with known potentials. Using these wave functions for the total capture cross section, we finally obtain[10]

$$\sigma_c(J)=\frac{8\pi K^{2J+1}}{\hbar^2 q^3}\frac{\mu}{(2S_1+1)(2S_2+1)}\frac{J+1}{J[(2J+1)!!]^2}\times\sum_{\substack{L_i,L_f\\J_i,J_f}}|T_J(N)|^2, \tag{5}$$

where

$$T_J(E)=A_J I_J P_J+(B_{1J}N_{1J}+B_{2J}N_{2J})I_J,$$

$$T_J(M)+C_J I_{J-1}G_J+(D_{1J}N_{1J}+D_{2J}N_{2J})I_{J-1},$$

$$P_J=\sqrt{4\pi}\langle J_f L_f S\|Y_J\|J_i L_i S\rangle=(-1)^{J+S+L_i+L_f}(L_i 0 J 0|L_f 0)$$

$$\sqrt{(2J_i+1)(2J_f+1)(2J+1)(2L_i+1)}\begin{Bmatrix} L_i & S & J_i \\ J_f & J & L_f \end{Bmatrix},$$

$$G_J=\sqrt{4\pi}\langle J_fL_fS\|\hat{L}Y_J^k\|J_iL_iS\rangle$$
$$=(-1)^{S+L_i+J_i}(L_i0k0|L_f0)(2L_i+1)$$
$$\times\sqrt{L_i(2L_i+1)(2k+1)(2J_i+1)(2J_f+1)(2J+1)}$$
$$\times\begin{Bmatrix} L_i & I & L_i \\ k & L_f & J \end{Bmatrix}\begin{Bmatrix} S & L_i & J_i \\ J & J_f & L_f \end{Bmatrix},$$

$$N_J=\sqrt{4\pi}\langle J_fL_fS\|\hat{S}Y_J^k\|J_iL_iS\rangle=$$
$$(-1)^{k+1-J+L_i+L_f+2S-J_i-J_f}(L_i0k0|L_f0)$$
$$\times\begin{Bmatrix} S & I & S \\ L_i & k & L_f \\ J_i & J & J_f \end{Bmatrix}$$
$$\times\sqrt{S(S+1)(2S+1)(2k+1)(2L_i+1)(2J_i+1)(2J_f+1)},$$

and I_J are radial integrals of the form

$$I_J=\langle L_f|R^J|L_i\rangle.$$

In these expressions all quantities are calculated analytically, except for the radial integrals, which are found numerically from the bound-state and scattering wave functions obtained by solving the Schrödinger equation. The asymptote of the radial scattering wave function is written as

$$R_{LJ}\to F_L(qr)\cos(\delta_{LJ})+G_L(qr)\sin(\delta_{LJ}), \tag{6}$$

where F_L and G_L are the Coulomb wave functions and δ_{LJ} are the phase shifts.

It is quite difficult to obtain the bound-state wave function numerically at distances of order 20–30 F. Therefore, at 10–20 F the numerical solution for the bound state was matched to the asymptote of the Whittaker function

$$R_{LJ}=\frac{\sqrt{2K_0}}{r}C_0W_{L\eta}(2K_0r),$$

$$W_{L\eta}(2K_0r)=(2K_0r)^{\eta}\exp(-K_0r), \tag{7}$$

where η is the Coulomb parameter, K_0 is the wave number determined by the binding energy, and C_0 is the asymptotic constant.

Equation (3) can also be used to calculate some static electromagnetic characteristics of nuclei. In particular, for the quadrupole, magnetic, and octupole moments and the reduced probabilities for radiative transitions, in the two-cluster model for ^{7}Li with $J_0=3/2^-$ we have

$$Q=-\frac{2}{5}YI_2=-\frac{2}{5}\frac{34}{49}I_2, \quad Y=(Z_1M_2^2+Z_2M_1^2)/M^2,$$

$$\frac{\mu}{\mu_0}=X+\mu_1=\frac{17}{42}+\mu_1,$$

$$X=\frac{1}{M}\left(\frac{Z_1M_2}{M_1}+\frac{Z_2M_1}{M_2}\right), \quad \frac{\Omega}{\mu}=\frac{3}{5}\frac{M_2^2}{M^2}I_2=\frac{48}{245}I_2, \tag{8}$$

$$B(M1)=\frac{1}{4\pi}(2\mu_1-X)^2I_0^2=\frac{1}{4\pi}(3\mu_1-\mu)^2I_0^2,$$

$$B(E2)=\frac{1}{4\pi}Y^2I_2^2.$$

Here the first cluster is assumed to be a triton or ^{3}He, which possess a magnetic moment, and $\mu_0=e\hbar/2m_0c$ is the nuclear magneton.

The magnetic and charge radii in the cluster model are given by[3,13]

$$\mu R_m^2=\frac{4}{21}\langle r_i^2\rangle+\frac{3}{14}\langle r_i^2\rangle+\mu_t\langle r_{tm}^2\rangle+\left(\frac{209}{3430}+\frac{432}{1225}\mu_t\right)I_2,$$

$$R_r^2=\frac{M_1}{M}\langle r_1^2\rangle+\frac{M_2}{M}\langle r_2^2\rangle+\frac{M_1M_2}{M^2}I_2, \tag{9}$$

where M_i and M are the masses of the clusters and the nucleus, $\langle r_i\rangle$ are the cluster radii, and the integral I_2 was defined below Eq. (5).

The Coulomb form factors were calculated using the results of Ref. 3, where it was shown that the form factor can be written as

$$F_J^2=\frac{1}{Z^2}V_J^2B_J,$$

$$B_J=(2J_f+1)(2J+1)(2L_i+1)$$
$$\times(L_i0J0|L_f0)^2\begin{Bmatrix} L_i & S & J_i \\ J_f & J & L_f \end{Bmatrix}^2, \tag{10}$$

where $L_{i,f}$ and $J_{i,f}$ are the orbital and total angular momenta of the initial i and final f states of the nucleus; J is the multipole order of the form factor; Z is the nuclear charge;

$$V_J=Z_1F_1I_{2J}+Z_2F_2I_{1J}; \tag{11}$$

Z_k and F_k are the charges and form factors of the kth cluster; and $I_{k,J}$ are the radial matrix elements corresponding to spherical Bessel functions between the initial and final states:

$$I_{k,J}=\langle L_fJ_f|j_J(g_kr)|L_iJ_i\rangle, \tag{12}$$

where $k=1,2$, $g_k=(M_k/M)q$, q is the momentum transfer, and $j_J(g_k,r)$ is the spherical Bessel function.

In the calculation of the form factors, the wave functions for scattering at resonance energies were normalized to the asymptotic form[14]

$$U_L=\exp(-\delta_L)(F_L\cos(\delta_L)+G_L\sin(\delta_L)). \tag{13}$$

The $E2$-transition probability and the charge radius can be determined using the Coulomb form factors:[3]

$$B(E2)=\frac{225Z^2}{4\pi}\lim_{q\to0}\left(\frac{F_2^2}{q^4}\right), \quad R_f^2=6\lim_{q\to0}\left(\frac{1-F(q)}{q^2}\right). \tag{14}$$

The wave functions of the ground and resonance states in the two-cluster system were found using the finite-difference method and the variational method of solving the radial Schrödinger equation[3]

$$U_L^n+(k^2-V(r))U_L=0. \tag{15}$$

The wave functions in the matrix elements (12) for the ground and resonance states can be represented as expansions in Gaussians:[3,15]

$$|LJ\rangle=R_L=r^L\sum_i C_i \exp(-\gamma_i r^2), \tag{16}$$

where the variational parameters γ_i and expansion coefficients C_i are found by the variational method for bound states or, for resonance states, by approximating the numerical wave functions as Gaussians.[15] In this case the matrix elements (12) are calculated analytically.[3]

2. THE CLASSIFICATION OF CLUSTER STATES

As an example, let us consider the classification of states in the N^2H system in the form given in Table I. Here the spin of the system can be 1/2 or 3/2, and the isospin is 1/2. The spin and isospin wave functions are characterized by definite Young schemes $\{f\}_S$ and $\{f\}_T$, which specify their symmetry under permutations of the corresponding nucleon coordinates.[5] For example, the spin symmetry is characterized by the $\{3\}_S$ scheme for $S=3/2$ and the $\{21\}_S$ scheme for $S=1/2$, and the isospin symmetry by the $\{21\}_T$ scheme. Since the symmetry of the spin–isospin wave function is determined by the direct inner product $\{f\}_{ST}=\{f\}_S\otimes\{f\}_T$ (Ref. 5), in the doublet channel we have $\{f\}_{ST}=\{1^3\}+\{21\}+\{3\}$ (Ref. 16). In the quartet channel this product gives only one scheme $\{21\}_{ST}$. The symmetry of the total wave function taking into account its orbital component is defined analogously: $\{f\}=\{f\}_L\otimes\{f\}_{ST}$. The total wave function of the system vanishes identically upon antisymmetrization except when it contains the antisymmetric component $\{1^N\}$, which is realized in the product of conjugate $\{f\}_L$ and $\{f\}_{ST}$. Therefore, schemes $\{f\}_L$ conjugate to $\{f\}_{ST}$ are assumed to be allowed in this channel. The possible orbital Young schemes in a system of $N=n_1+n_2$ particles can be determined using the Littlewood theorem[5] as the direct outer product of the orbital schemes of each of the subsystems, which in this case gives $\{f\}_L=\{2\}\times\{1\}=\{21\}_L+\{3\}_L$. Here the scheme $\{2\}$ corresponds to the deuteron with $LS=01$. From this we see that in the quartet channel only the orbital wave function with symmetry $\{21\}_L$ is allowed. The function with $\{3\}_L$ is forbidden because the product $\{21\}_{ST}\otimes\{3\}_L$ does not lead to an antisymmetric component of the wave function. In the doublet channel we have $\{3\}_{ST}\otimes\{1^3\}_L=\{1^3\}$ and $\{21\}_{ST}\otimes\{21\}_L=\{1^3\}$, and in both cases we obtain an antisymmetric scheme. The two possible Young orbital schemes $\{21\}_L$ and $\{3\}_L$ are thereby allowed in the doublet channel.[6,7]

It is this result which explains the mixing in orbital schemes in states with definite $ST=1/21/2$ for any L. Therefore, the doublet S-wave interaction potential obtained from the experimental phase shifts effectively depends on both orbital schemes, while the ground state corresponds to the pure symmetry $\{3\}_L$. This means that these potentials are different in the N^2H system, and from the scattering interactions $V^{\{3\}+\{21\}}$ it is necessary to isolate the component $V^{\{3\}}$, which is in principle applicable for calculating the ground-state characteristics.[6–8] In particular, when performing calculations for photoprocesses the bound states can be described using a potential which is pure in the Young schemes, while scattering states, for example, the final states of photodisintegration, can be described using the potential obtained directly from the experimental phase shifts.

As mentioned above, the experimental phase shifts of the doublet channel can be represented as half the sum of the pure phase shifts with the schemes $\{21\}_L$ and $\{3\}_L$. If we assume that quartet phase shifts which are pure in the orbital schemes $\{21\}_L$ can be used as the doublet phase shifts with $\{21\}_L$, then it is also easy to find the pure doublet phase shifts with $\{3\}_L$ and then use them to parametrize the pure interactions.

The complete classification of the allowed and forbidden states of light cluster systems is given in Table I (Ref. 9).

3. INTERCLUSTER POTENTIALS AND BOUND-STATE CHARACTERISTICS

The scattering and bound-state wave functions were calculated using central Gaussian potentials of the form[10]

$$V(r)=-V_0\exp(-\alpha r^2)+V_c(r),$$

$$V_c(r)=\begin{cases}\dfrac{Z_1Z_2}{r}, & r>R_c,\\[2ex] Z_1Z_2\left(3-\dfrac{r^2}{R_c^2}\right)\Big/\,2R_c, & r<R_c.\end{cases} \tag{17}$$

In some cases a peripheral repulsive interaction $V_i\exp(-\beta r)$ was added to these, as it is necessary for correctly describing the negative values of the D- or F-wave phase shifts at low energies if the S- and P-wave phase shifts are positive. The potentials were reconstructed from the phase shifts of cluster scattering so that one partial wave is described by one Gaussian with known parameters in a maximally wide energy range.

First, we shall consider the intercluster interaction potentials and characteristics of cluster nuclei for the pure systems p^3He, n^3H, ^{4}He^{3}H, ^{4}He^{3}He, ^{4}He^{2}H, and ^{3}He^{3}H, and then we will study potentials corresponding to mixed Young schemes.

3.1. The ^{4}He^{2}H, ^{3}He^{3}H, and ^{4}He^{3}H cluster systems

We see from Table I that the orbital states in the ^{4}He^{2}H, ^{4}He^{3}H, ^{4}He^{3}He and ^{3}He^{3}H systems for the nuclei ^{6}Li and ^{7}Li, ^{7}Be are pure in their Young schemes. Therefore, the potentials obtained from the phase shifts can be used to study the bound-state characteristics. The results will depend only on the degree of clusterization of the nuclei in the cluster channels. Since the clusterization probability of these nuclei is relatively high, the results of the calculations should on the whole reproduce the experimental data. The interaction parameters for pure states in ^{6}Li and ^{7}Li obtained in Refs. 3

TABLE I. Classification of allowed and forbidden states in light cluster systems. L is the orbital angular momentum for the bound states.

System	T	S	$\{f\}_S$	$\{f\}_T$	$\{f\}_{ST}$	$\{f\}_L$	L	$\{f\}_{PC}$	$\{f\}_{3C}$
N^2H	1/2	1/2	{21}	{21}	{111}+{21}+{3}	{3}	0	{3}	-
						{21}	1	{21}	-
		3/2	{3}	{21}	{21}	{3}	0	-	{3}
						{21}	1	{21}	-
n^3He	0	0	{22}	{22}	{4}+{22}+{1111}	{4}	0	{4}	-
p^3H						{31}	1	-	{31}
		1	{31}	{22}	{31}+{211}	{4}	0	-	{4}
						{31}	1	{31}	-
p^3He	1	0	{22}	{31}	{31}+{211}	{4}	0	-	{4}
n^3H						{31}	1	{31}	-
p^3H		1	{31}	{31}	{4}+{31}+{22}	{4}	0	-	{4}
n^3He					+{211}	{31}	1	{31}	-
$^2H^2H$	0	0	{22}	{22}	{4}+{22}+{1111}	{4}	0	{4}	-
						{31}	1	-	{31}
						{22}	0,2	{22}	-
		1	{31}	{22}	{31}+{211}	{4}	0	-	{4}
						{31}	1	{31}	-
						{22}	0,2	-	{22}
		2	{4}	{22}	{22}	{4}	0	-	{4}
						{31}	1	-	{31}
						{22}	0,2	{22}	-
$^2H^3He$	1/2	1/2	{32}	{32}	{5}+{41}+{32}	{5}	0	-	{5}
					+{311}+{221}	{41}	1	{41}	-
$^2H^3H$					+{2111}	{32}	0,2	{32}	-
		3/2	{41}	{32}	{41}+{32}+{311}	{5}	0	-	{5}
					+{221}	{41}	1	-	{41}
						{32}	0,2	{32}	-
p^4He	1/2	1/2	{32}	{32}	{5}+{41}+{32}	{5}	0	-	{5}
n^4He					+{311}+{221}	{41}	1	{41}	-
					+{2111}				
$^4He^2H$	0	1	{42}	{33}	{51}+{411}+{33}	{6}	0	-	{6}
					+{321}+{2211}	{51}	1	-	{51}
						{42}	0,2	{42}	-
$^3He^3H$	0	0	{33}	{33}	{42}+{222}+{6}	{6}	0	-	{6}
					+{3111}	{51}	1	-	{51}
						{42}	0,2	-	{42}
						{33}	1,3	{33}	-
		1	{42}	{33}	{51}+{411}+{33}	{6}	0	-	{6}
					+{321}+{2211}	{51}	1	-	{51}
						{42}	0,2	{42}	-
						{33}	1,3	-	{33}
$^3H^3H$	1	0	{33}	{42}	{51}+{411}+{33}	{6}	0	-	{6}
$^3He^3He$					+{321}+{2211}	{51}	1	-	{51}
$^3He^3H$						{42}	0,2	{42}	-
						{33}	1,3	-	{33}
		1	{42}	{42}	{6}+2{42}+{51}	{6}	0	-	{6}
					+{411}+2{321}	{51}	1	-	{51}
					+{222}+{3111}	{42}	0.2	-	{42}
						{33}	1,3	{33}	-
$^4He^3H$	1/2	1/2	{43}	{43}	{7}+{61}+{52}	{7}	0	-	{7}
					+{511}+{43}	{61}	1	-	{61}
					+{421}+{4111}	{52}	0,2	-	{52}
					+{322}+{3211}	{43}	1,3	{43}	-
					+{2221}+{331}				
n^6Li	1/2	1/2	{43}	{43}	{7}+{61}+{52}	{7}	0	-	{7}
p^6Li					+{511}+{43}	{61}	1	-	{61}
					+{421}+{4111}	{52}	0,2	-	{52}
					+{322}+{3211}	{43}	1,3	{43}	-
					+{2221}+{331}	{421}	1,2	{421}	-
		3/2	{52}	{43}	{61}+{52}+{511}	{7}	0	-	{7}
					+{43}+2{421}	{61}	1	-	{61}
					+{331}+{322}	{52}	0,2	-	{52}
					+{3211}	{43}	1,3	-	{43}
						{421}	1,2	{421}	-
$^4He^4He$	0	0	{44}	{44}	{8}+{62}+{5111}	{8}	0	-	{8}
					+{44}+{422}	{71}	1	-	{71}
					+{3311}+{2222}	{62}	0,2	-	{62}

TABLE 1. (*Continued.*)

System	T	S	$\{f\}_S$	$\{f\}_T$	$\{f\}_{ST}$	$\{f\}_L$	L	$\{f\}_{PC}$	$\{f\}_{3C}$
						{53}	1,3	-	{53}
						{44}	0,2,4	{44}	-
p^7Li	0	1	{53}	{44}	{71}+{611}+{53}	{8}	0	-	{8}
					+{521}+{431}	{71}	1	-	{71}
					+{4211}+{332}	{53}	1,3	-	{53}
					+{3221}	{44}	0,2,4	-	{44}
						{431}	1,2,3	{431}	-
		2	{62}	{44}	{62}+{521}+{44}	{8}	0	-	{8}
					+{431}+{422}	{71}	1	-	{71}
					+{3311}	{53}	1,3	-	{53}
						{44}	0,2,4	-	{44}
						{431}	1,2,3	-	{431}
n^7Li	1	1	{53}	{53}	{8}+2{62}+{71}	{8}	0	-	{8}
p^7Li					+{611}+{53}+{44}	{71}	1	-	{71}
					+2{521}+{5111}	{53}	1,3	-	{53}
					+{44}+{332}	{44}	0,2,4	-	{44}
					+2{431}+2{422}	{431}	1,2,3	{431}	-
					+{4211}+{3311}				
					+{3221}				
		2	{62}	{53}	{71}+{62}+{611}	{8}	0	-	{8}
					+2{53}+2{521}	{71}	1	-	{71}
					+2{431}+{422}	{53}	1,3	-	{53}
					+{4211}+{332}	{44}	0,2,4	-	{44}
						{431}	1,2,3	-	{431}
^{2}H^{6}Li	0	0	{44}	{44}	{8}+{62}+{5111}	{8}	0	-	{8}
					+{44}+{422}	{71}	1	-	{71}
					+{3311}+{2222}	{62}	0,2	-	{62}
						{53}	1,3	-	{53}
						{521}	1,2	-	{521}
						{44}	0,2,4	{44}	-
						{431}	1,2,3	-	{431}
						{422}	0,2	{422}	-
		1	{53}	{44}	{71}+{611}+{53}	{8}	0	-	{8}
					+{521}+{431}	{71}	1	-	{71}
					+{4211}+{332}	{62}	0,2	-	{62}
					+{3221}	{53}	1,3	-	{53}
						{521}	1,2	-	{521}
						{44}	0,2,4	-	{44}
						{431}	1,2,3	{431}	-
						{422}	0,2	-	{422}
		2	{62}	{44}	{62}+{521}+{44}	{8}	0	-	{8}
					+{431}+{422}	{71}	1	-	{71}
					+{3311}	{62}	0,2	-	{62}
						{53}	1,3	-	{53}
						{521}	1,2	-	{521}
						{44}	0,2,4	-	{44}
						{431}	1,2,3	-	{431}
						{422}	0,2	{422}	-

and 10 are given in Table II. The interactions in the ^{4}He^{3}H and ^{4}He^{3}He systems differ only by the Coulomb term.

Owing to the lack of experimental data, for the ^{3}He^{3}He system the potentials were constructed exclusively from resonating-group calculations of the phase shifts.[17] The parameters of these interactions coincide with those of ^{3}He^{3}H for $S=0$; however, here even L correspond only to $S=0$, and odd L correspond to $S=1$.

The quality of the description of the phase shifts is shown in Figs. 1–4 together with the experimental data from Ref. 18 for ^{4}He^{2}H, from Refs. 19 and 20 for ^{4}He^{3}H, and from Ref. 21 for ^{3}He^{3}H. In Figs. 3 and 4 the crosses show the calculated ^{3}He^{3}H phase shifts obtained using the resonating-group method.[22] The triplet ^{3}He^{3}H potentials given in Table II, whose the phase shifts are shown by the solid lines in Fig. 3a, incorrectly reproduce the bound-state energy of ^{6}Li. To obtain the correct value of -15.8 MeV for the ground state it is necessary to increase the interaction depth to 105 MeV. The description of the energy of the D_3 level requires a potential of depth 107.5 MeV. The phase shifts of these potentials are shown by the dashed lines in Fig. 3a.

The ^{4}He^{2}H potential in the D_3 wave allows a phase shift of 90° to be obtained at energy 0.71 MeV, in good agreement with the data of Ref. 23, where the value 0.711 MeV is quoted. On the whole, the elastic cross sections for ^{3}He^{3}H

TABLE II. Parameters of the potentials for $^4He^3H$, $^4He^3He$, $^4He^2H$, and $^3He^3H$ scattering. For the $^4He^3H$ and $^4He^3He$ systems $\alpha=0.15747\ F^{-2}$ and $R_c=3.095$ F. For $^4He^2H$ and $^3He^3H$, $R_c=0$ F.

$^7Li(^7Be)$		$^6Li(^4He^2H)$			$^6Li(^3He^3H)$			
					$S=1$		$S=0$	
L_J	V_0 (MeV)	L_J	V_0 (MeV)	α (F^{-2})	V_0 (MeV)	α (F^{-2})	V_0 (MeV)	α (F^{-2})
S	67.5	S	76.12	0.2	90	0.18	85.0	0.18
$P_{1/2}$	81.92	P_0	68.0	0.22	52.5	0.2		
$P_{3/2}$	83.83	P_1	79.0	0.22	65.0	0.2	74.0	0.2
$D_{3/2}$	66.0	P_2	85.0	0.22	80.0	0.2		
$D_{5/2}$	69.0	D_1	63.0	0.19	72.0	0.18		
$F_{5/2}$	75.9	D_2	69.0	0.19	85.0	0.18	85.0	0.18
$F_{7/2}$	84.8	D_3	80.88	0.19	90.0	0.18		

scattering at the energies 5.79 MeV and 19.91 MeV agree with the experimental data of Refs. 21 and 24.

The cluster interactions obtained from the phase shifts were used to calculate various characteristics of the nuclear ground states. Here the clusters were associated with the properties of the corresponding nuclei in the free state. In particular, the nuclear charge radius was found using the following cluster radii: 1.9660(68) F for ^2H, 1.68(3) F for ^3H, 1.844(45) F for ^3He, and 1.673(1) F for ^4He (taken from Ref. 25). The magnetic radius of ^3H was taken to be 1.72(6) F (Ref. 25). The proton radius was taken to be 0.805(11) F.

The calculated charge radii, the binding energies in cluster channels, the magnetic, quadrupole, and octupole moments, the probabilities for $\frac{1}{2}^- \to \frac{3}{2}^-$ transitions in ^7Li and the $1^+ \to 3^+$ transition in ^6Li, and the asymptotic constants are given in Table III together with the experimental values from Refs. 26–29, the calculations using the resonating-group method (RGM),[12,30] and the cluster-model calculations.[13,31] In Fig. 5 we show the cluster momentum distributions for ^6Li in the $^4He^2H$ and $^3He^3H$ models, together with the experimental values.[32]

Equation (11) for V_L contains not only the matrix elements, but also the form factors of the clusters. The form factors of the corresponding nuclei in the free state were used for the latter. Parametrizations of these form factors can be found in Refs. 3 and 26. For example, for ^4He we can use an expression of the form

$$F=(i-(aq^2)^n)\exp(-bq^2), \tag{18}$$

where $a=0.09986$, $b=0.46376$, and $n=6$. For ^3H and ^3He we can also use (18), but with the parameters $a=0.0785$,

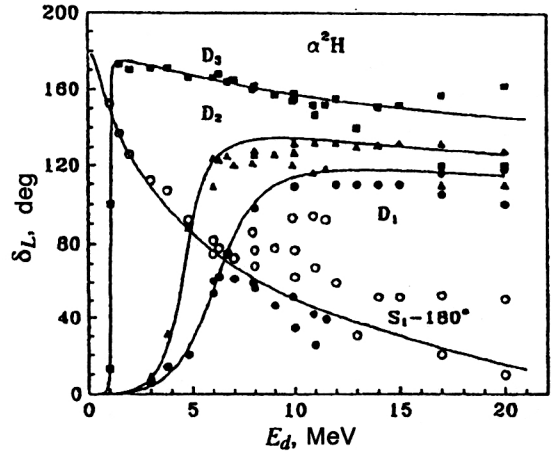

FIG. 1. Phase shifts of elastic $^4He^2H$ scattering. The curves are calculated for the potentials with the parameters in Table II. The points, triangles, crosses, and squares are the experimental data of Ref. 18.

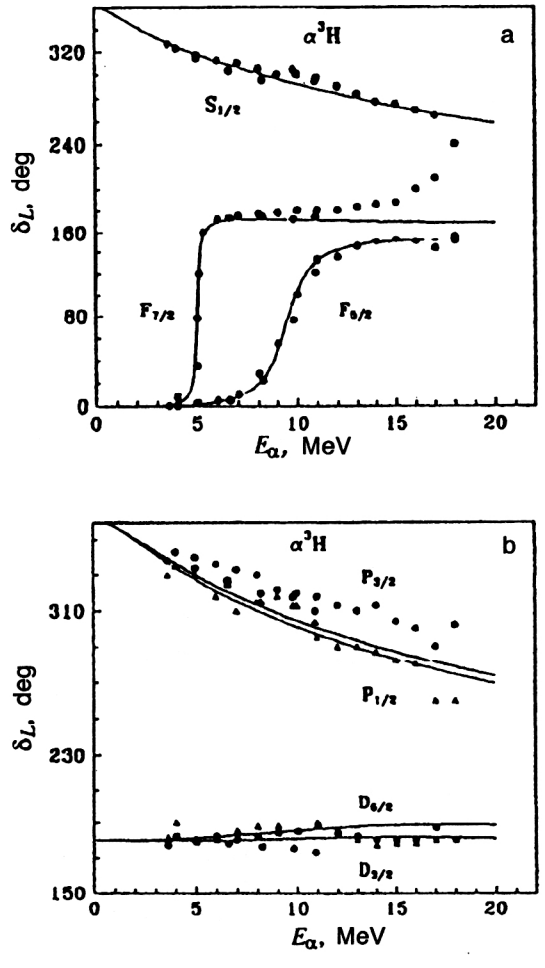

FIG. 2. Phase shifts of elastic $^4He^3H$ scattering. The curves are calculated for the potentials with the parameters in Table II. The points and triangles are the experimental data of Refs. 19 and 20.

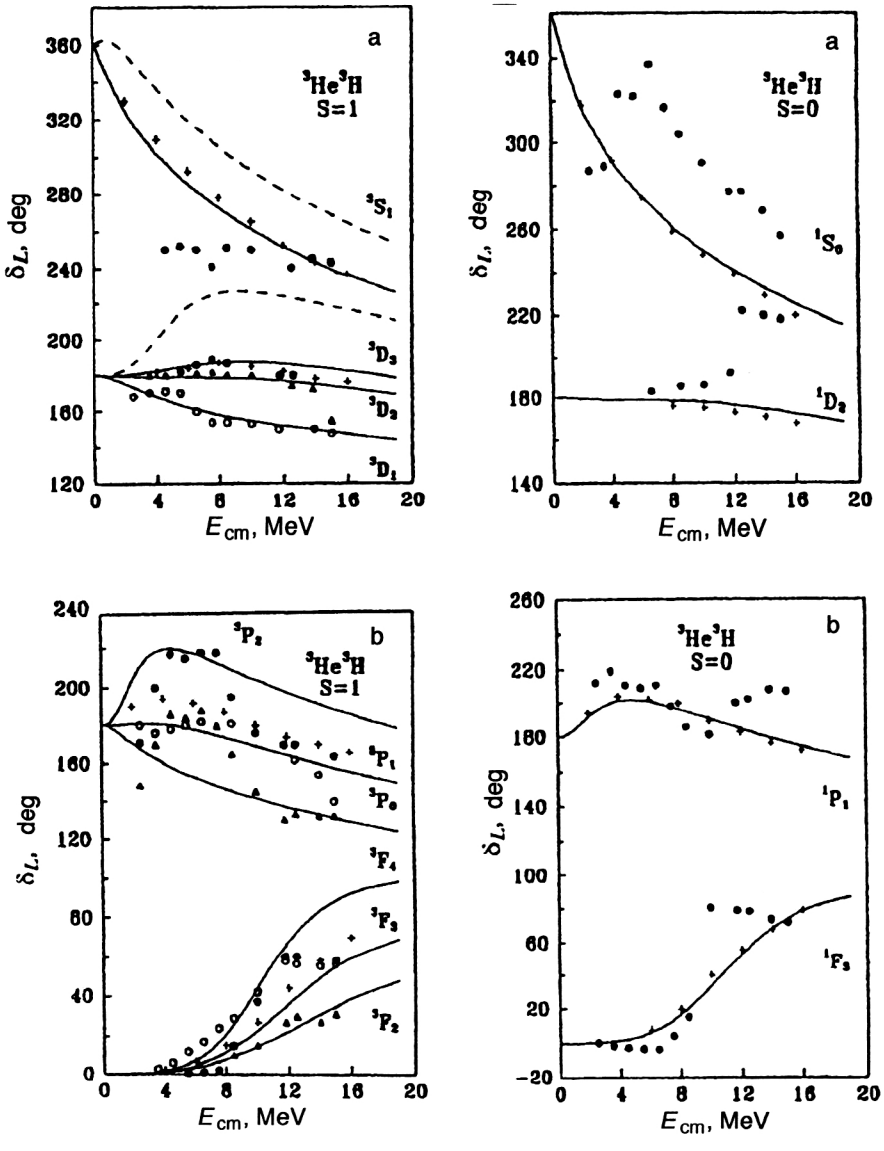

FIG. 3-4. Phase shifts of elastic ^{3}He^{3}H scattering. The curves are calculated for the potentials with the parameters in Table II. The points, triangles, and circles are the experimental data of Ref. 21. The crosses are the RGM calculations of Ref. 22.

$b=0.4075$, $n=5.46$ and $a=0.0872$, $b=0.481$, $n=7.9$, respectively. The parametrization of the deuteron form factor is

$$F=\exp(-aq^2)+bq^2\exp(-cq^2) \tag{19}$$

with the parameters $a=0.49029$, $b=0.01615$, and $c=0.16075$. These expressions give the correct behavior of the form factors for momenta up to $20\,F^{-2}$, which is quite sufficient, because the form factors of these nuclei have been measured only up to $3.5-4.5\,F^{-1}$. The usual Gaussian parametrization with $a=0.0864\,F^2$ was used for the proton form factor.[33]

The Coulomb form factors of lithium nuclei have been studied by many authors using the resonating-group method (RGM),[34–36] various phenomenological approaches,[14,37,38] and the cluster model.[39] The RGM calculations of the elastic and inelastic form factors of ^{7}Li give a good description of the experimental data at small momentum transfers of order $7-8\,F^{-2}$ (Ref. 35). However, at $3-4\,F^{-1}$ a second maximum is observed experimentally,[40] and it is not present in the RGM calculations.[34,35] In the case of the ^{6}Li nucleus, the existing RGM results taking into account distortions or complete antisymmetrization give a generally good reproduction of the shape of the second maximum of the elastic form factor.[36] Phenomenological wave functions of the ^{6}Li nucleus were used in Refs. 14, 37, and 38, and a better description of the elastic and inelastic 3^+ form factors was obtained at low momenta. The second maximum in the elastic Coulomb form factor of ^{6}Li can also be reproduced by a three-body model of the nucleus[41] using potentials with forbidden states.

In Ref. 3 the form factors were calculated in the two-cluster model using Eqs. (10)–(12), (18), and (19). The results for the elastic form factor of ^{6}Li (Ref. 3) are shown by the solid line in Fig. 6a together with the experimental data.[40] The dashed line is the data of Ref. 35 obtained by RGM calculations, and the dot–dash line shows the results of the three-body calculations.[41] We see that in the region $3-4\,F^{-1}$ the calculated curve lies slightly below the experimental data, nearly coinciding with the three-body calculations, and that it has no clear minimum at intermediate momenta. The latter fact is due to the smooth behavior of the deuteron form

TABLE III. Calculated electromagnetic characteristics of the nuclei ^{7}Li, ^{7}Be, and ^{6}Li.

	^{7}Li			
	Calculation	Exp. (Refs. 26–29)	RGM (Refs. 12, 30)	Calculation (Refs. 13, 31)
Q (mb)	−38.2	−36.6(3);40.6(3)	−34.2–41.9	−37.4
μ (μ_0)	3.383	3.2564	2.79–3.16	3.384
Ω/μ (F^2)	2.70	2.4(5);2.9(1)	3.23.6	2.48
$B(M1)$ (μ_0^2)	2.45	2.48(12)	1.96–2.17	2.45
$B(E2)$ (e^2 F^4)	7.3	7.42(14)–8.3(6)	5.4–11.3	7.0
E_0 (MeV)	−2.47	−2.467		
E_1 (MeV)	−1.99	−1.989		
R_f (F)	2.40	2.39(3)		
R_m (F)	2.77	2.70(15);2.98(5)		
C_0	3.9	—		
	^{7}Be			
	Calculation	Exp. (Refs. 26–29)	RGM (Refs. 12, 30)	Calculation (Refs. 13, 31)
Q (mb)	−59.3		−58.4	
μ (μ_0)	−1.532		−1.27	−1.533
Ω/μ (F^2)	2.85		4.71	
$B(M1)$ (μ_0^2)	1.87	1.87(25)	1.58	1.87
$B(E2)$ (e^2 F^4)	17.5		17.0	
E_0 (MeV)	−1.60	−1.586		
E_1 (MeV)	−1.14	−1.157		
	^{6}Li			
	Calculation		Exp. (Refs. 26–29)	
E (MeV)	−1.472		−1.4735	
R_f (F)	2.56		2.54(5)	
C_0	3.22(2)		2.9–3.6	
$B(E2)$ (e^2 F^4)	25.1		25.6	

factor, which has no minimum in this range of momentum transfers. In our calculations we did not use any deformation of the deuteron; however, this is justified only for 100% clusterization of the nucleus in the ^{4}He^{2}H channel. Since the clusterization probability is apparently less than 60–80%, the model without distortions represents an approximation to the actual situation. Finally, deformations or distortions of the deuteron cluster can also be introduced in the ^{4}He^{2}H model. However, here there is a fitted parameter characterizing the degree of compression of the deuteron. Meanwhile, the probability of deuteron clusterization in the nucleus can be judged from the calculations without cluster deformation. For 100% clusterization all the results obtained using the simple two-cluster model should apparently be in good agreement with experiment. Any deviation of the calculated characteristics from the experimental data will indicate less clusterization, when the cluster can no longer be completely associated with the characteristics of the corresponding nucleus in the free state. The deviation of the elastic form factor from experiment, primarily at intermediate momenta, directly indicates that the model without deformation is an approximation. The smaller value of the form factor at $3-4\,\mathrm{F}^{-1}$ is due to the absence of the D wave in the nuclear wave function. It can be introduced only by taking into account the tensor component in the interaction potential.

In Fig. 6b the solid line shows the inelastic form factor with transition to the 3^+ level, compared with the results of Ref. 41 for three-body wave functions. We see that the calculation practically coincides with experiment,[14,38] and has the second maximum. In contrast to the calculations of the elastic form factor, the inelastic form factor turns out to be very sensitive to the depth and shape of the potential. For example, a change of the depth by 0.03–0.05 MeV has practically no effect on the behavior of the 3^+ phase shift, but it causes the form factor to change by a factor of 2 to 3. To correctly describe this form factor it was necessary to slightly change the potential of the D_3 wave, using 80.93 MeV, which differs from the results given in Table II by 50 keV.

In Fig. 7a the solid line shows the calculated elastic Coulomb form factor of the ^{7}Li nucleus, which has a clear minimum at $3.2\,\mathrm{F}^{-1}$ and a rise at higher momenta lying practically in the range of experimental error.[40] Here the dashed line shows the RGM calculations of Ref. 35, where the calculated curve falls off smoothly. In Figs. 7b and 7c we show the inelastic Coulomb form factors with transition to the $\frac{1}{2}^-$ and $\frac{7}{2}^-$ levels. The dashed line is the result of Ref. 35. The form factor of the $\frac{1}{2}^-$ level is described up to the second maximum, where its value is clearly less than experiment. Similar results were also obtained for the $\frac{7}{2}^-$ form factor. Here there is a second maximum which is completely absent in the RGM calculations.[34,35] We note that the potentials from Table II without any changes of the parameters were used for the calculations.

3.2. The p^3He and n^3H cluster systems

The p^3He and n^3H cluster systems with pure isospin $T=1$ have only a single allowed orbital scheme {31} with

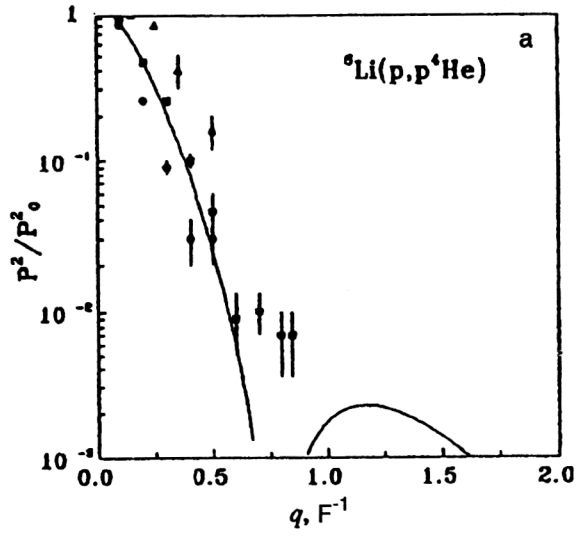

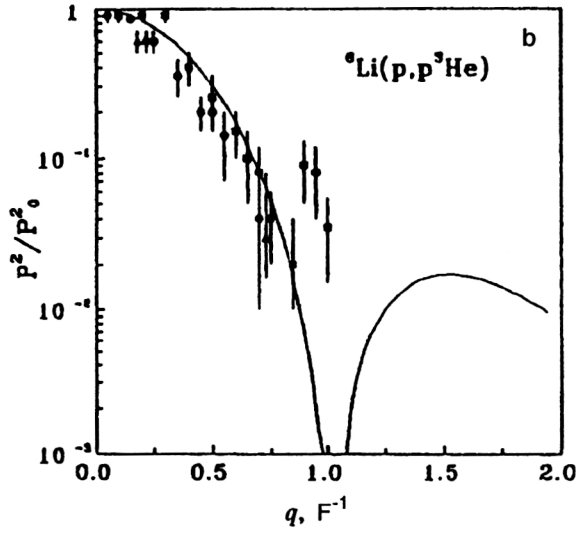

FIG. 5. Momentum distributions of ^{4}He^{2}H and ^{3}He^{3}H in the ^{6}Li nucleus. The curves are calculated for the potentials with the parameters in Table II. The points and squares are the experimental data of Ref. 32.

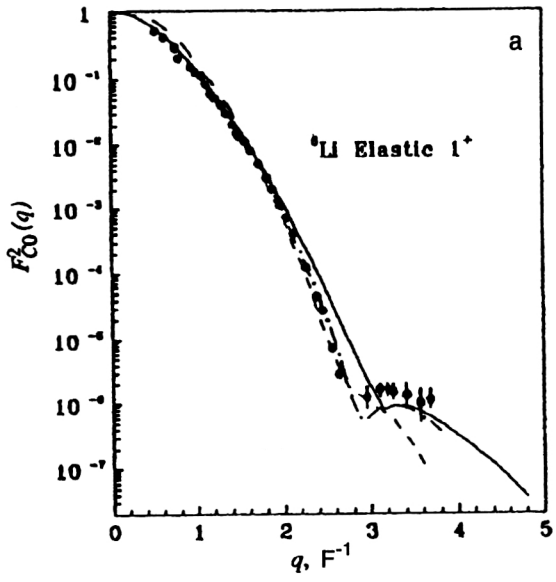

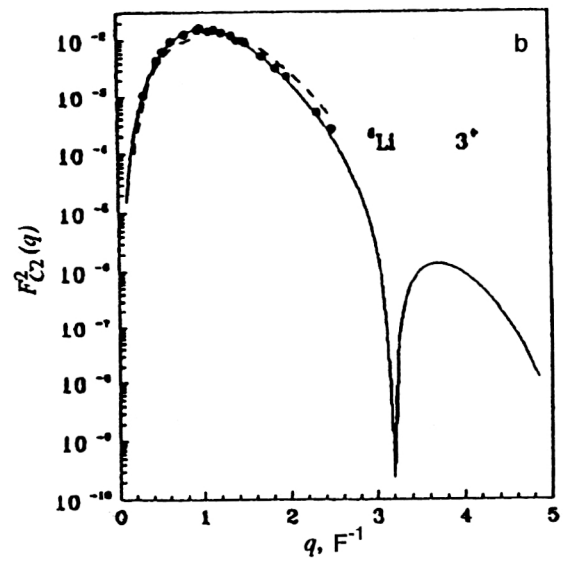

FIG. 6. Elastic and inelastic Coulomb form factors of the ^{6}Li nucleus with transition to the 3^+ level. The curves are the calculations using various models (explained in the text). The points are the experimental data of Refs. 38 and 40.

S-wave forbidden configuration {4} in the triplet and singlet states.

The phase-shift analysis at energies up to 1 MeV performed in Ref. 42 leads to a certain ambiguity in the phase shifts. Two sets of solutions noticeably differing from each other are obtained. There are two groups of studies[43,44] at energies of 2–14 MeV, where two sets of the results were also obtained for the singlet and triplet P-wave phase shifts with $J=1$. In Ref. 43 the singlet P_1 phase shift at energies of 6–12 MeV reaches about 40−50°, and the P_1 phase shift for $S=1$ reaches about 20−30°. In Ref. 44 the singlet phase shift is lower, 20−30°, and the triplet phase shift is higher, 40−50°. These two variants, referred to as solutions A and C, were studied in Ref. 45. The energy range above 18 MeV was studied in Ref. 46. In Table IV we give the p^3He interaction parameters[8] together with the energies of the forbidden states at $L=0$. In even waves they coincide with those given in Refs. 6 and 7.

In Figs. 8 and 9 the solid lines show the calculated phase shifts for these potentials, the points, squares, and vertical lines show the experimental data of Refs. 42, 43, and 45, and the triangles show the data of Ref. 44. The cross sections for elastic p^3He scattering at energies of 6.82 MeV and 10.77 MeV calculated using these potentials agree well with the experimental data.[42–45] In Fig. 10 we show the n^3H phase shifts and the data of Ref. 47. The crosses show the results of the RGM calculations from Ref. 48.

Since there are several different variants of the phase-shift analyses for the singlet P wave, the potential parameters given in Table IV were selected so as to obtain a compromise between the different analyses. The description of the data of Ref. 44, shown by the triangles, requires a poten-

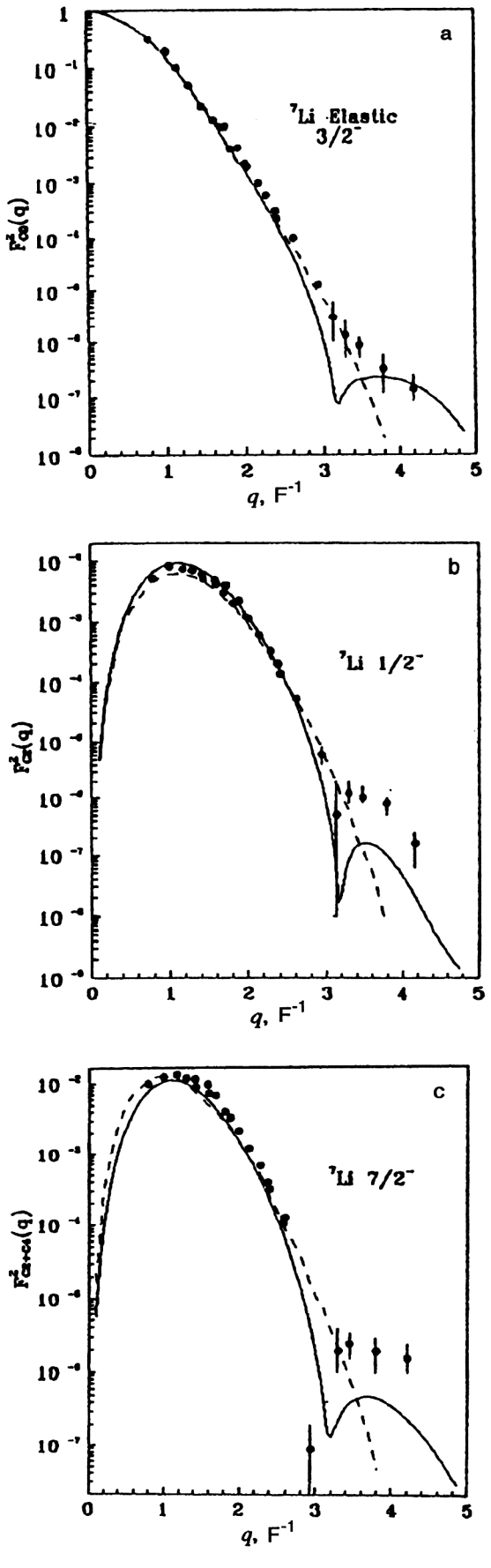

FIG. 7. Elastic and inelastic Coulomb form factors for the $\frac{1}{2}^-$ and $\frac{7}{2}^-$ levels of the ^{7}Li nucleus. The solid lines are the calculations using the cluster model with the potentials of Table II, the dashed lines are the RGM calculations of Ref. 35, and the points are the experimental data of Ref. 40.

tial with a depth of about 11 MeV (dotted line in Fig. 9), while the phase shifts of Ref. 43 are reproduced by a deeper interaction with $V_0=17$ MeV (dashed line). For describing the triplet P wave[44] the depth of the potential must be 17 MeV (dotted line in Fig. 8b), while for the data of Ref. 43 it must be 13 MeV (dashed line). The energies of forbidden states with the {4} scheme are given in Table IV, and the allowed states with symmetry {31} in P waves turn out to be unbound.

3.3. The N^2H cluster system

We see from Table I that only the {21} orbital scheme is possible in the quartet channel of the N^2H system, and the symmetry {3} is forbidden. However, the doublet channel is compatible with the two schemes {21} and {3}, and the potentials obtained using the phase shifts effectively depend on these Young schemes.

Experimental data on the phase-shift analysis in the p^2H system are available in a fairly wide energy range, and on the whole the results of different studies agree with each other.[49] These data were used to obtain the interaction potentials whose parameters are given in Table V.

In Fig. 11 we show the calculated and experimental[49] elastic p^2H phase shifts at low energies. The solid lines in Fig. 11a give the calculated phase shifts for even waves using the second set of parameters for the doublet potentials from Table V. The phase shifts corresponding to the first set of parameters are shown by the dashed lines and lead to a D-wave phase shift which is slightly too high. The solid line for the P wave shows the results obtained with the second set, and the dotted line gives the results obtained with the first set. In Fig. 11b the solid lines show the results for the potentials of Table V, and the dashed lines show the phase shifts for the interaction from Ref. 6 with the parameters $V_0=57$ MeV, $\alpha=0.37$ F^{-2}, $V_1=7.2$ MeV, and $\beta=0.36$ F^{-1} for even waves and $V_0=8.8$ MeV and $\alpha=0.06$ F^{-2} for odd waves. We see that these potentials are quite good at reproducing the energy behavior of the experimental phase shifts, and the calculated cross sections for elastic p^2H scattering at 2.5 and 10 MeV agree with the data of Refs. 49 and 50.

In Table V we give the bound-state energies for both spin states. In the quartet channel for $L=0$ there is a forbidden state with scheme {3}, and the allowed state with scheme {21} for $L=1$ is located in the continuum, just as in the case of the p^3He system. The mixed S-wave potential of the doublet channel leads to a bound state with energy different from the binding energy of the ^{3}He nucleus.

As mentioned above, the experimental mixed doublet phase shifts can be represented as half the sum of the pure phase shifts:

$$\delta_L^{\{f_1\}+\{f_2\}}=\frac{1}{2}\,\delta_L^{\{f_1\}}+\frac{1}{2}\,\delta_L^{\{f_2\}}. \tag{20}$$

In this case $\{f_1\}=\{3\}$ and $\{f_2\}=\{21\}$. If we assume that the quartet phase shifts of symmetry {21} can be used as the doublet phase shifts with the same symmetry {21}, then it is easy to find the pure doublet phase shifts with scheme {3}. In Fig. 11c the pure p^2H phase shifts obtained in this manner

TABLE IV. Interaction potentials of pure cluster p^3He and n^3H systems and bound-state energies E_{bs}. $R_c=0$ for the Coulomb potential. The energies for the n^3H system are given in parentheses.

L_J	V_0 (MeV)	α (F^{-2})	V_1 (MeV)	β (F^{-1})	E_{bs} (MeV)
$S=0$					
Even	110	0.37	45	0.67	−9.0(−11.4)
Odd	14.0	0.1			
$S=1$					
Even	43	0.26			−3.6(5.3)
P_0	10	0.1			
P_1	15	0.1			
P_2	20	0.1			

are shown by the vertical lines, which give the error range. The interaction parameters are given in Table VI together with the bound-state energies, and the calculated phase shifts are shown in Fig. 11c. In even waves the phase shifts of the potential with the first set of parameters are shown by the solid line. The dashed line gives the results for the second set of parameters, which are practically the same as those of Ref. 6. The phase shifts of the purely repulsive P-wave interaction are shown by the dotted line, and the solid line gives the phase shifts of the potential with peripheral repulsion from Ref. 6 with the parameters $V_0=13.8$ MeV, $\alpha=0.16$ F^{-2}, $V_1=1.6$ MeV, and $\beta=0.09$ F^{-1}.

We see from this figure that the behavior of the pure p^2H phase shift with $L=1$ is reproduced well. The S-wave phase shift has a nearly resonance behavior, and it is not possible to find an interaction capable of describing its shape and also the bound-state characteristics. These interactions for the ground states correctly describe the binding energies of ^{3}He and ^{3}H. The experimental values of the energies are −5.493 MeV and −6.257 MeV, respectively.

The two pure S-wave p^2H interaction potentials lead to practically identical phase shifts, but only the second one without any deformation of the deuteron cluster gives a relatively accurate Coulomb elastic form factor at small momenta. The ^{3}He charge radius for this interaction is $R_f=1.89$ F, and $R_r=2.08$ F, which is slightly larger than the experimental value. The asymptotic constant is 1.8(1), while the experimental values lie in the range 1.8–2.3 (Ref. 27). In the case of the n^2H system, the second potential slightly lowers the binding energy, but if the depth is decreased to 53.9 MeV, the energy turns out to be −6.25 MeV and the radii are $R_f=1.89$ F and $R_r=2.01$ F.

For the first potential variant, the description of the radius and form factor requires the introduction of a deuteron

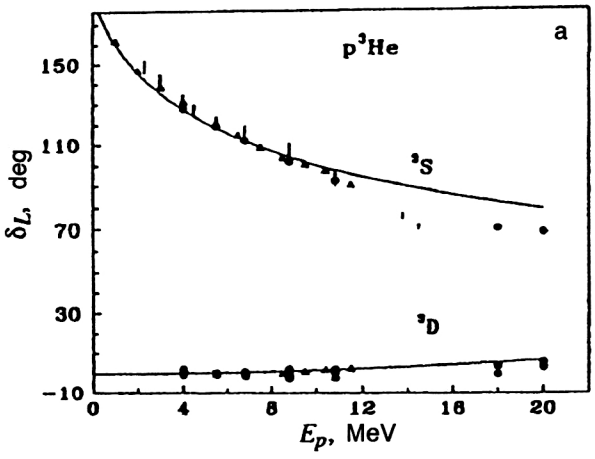

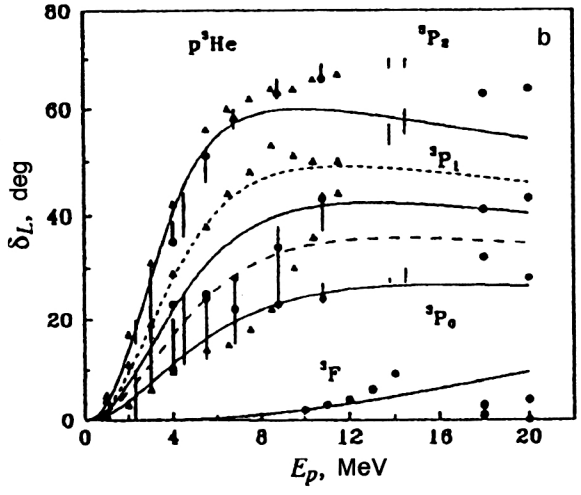

FIG. 8. Phase shifts of elastic p^3He scattering. The points, squares, and vertical lines are the experimental data,[42,43,45] and the triangles are from Ref. 44. The curves are the result of calculations using various potentials.

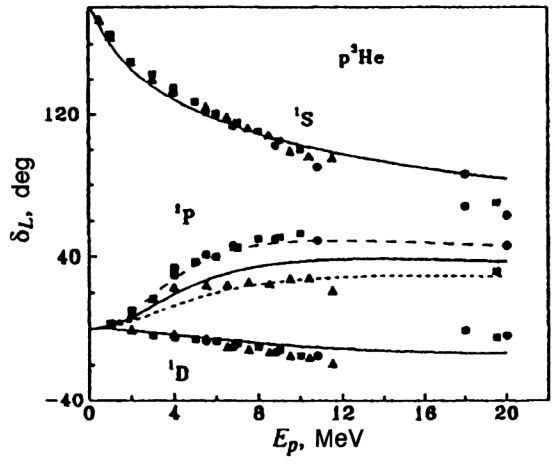

FIG. 9. Phase shifts of elastic p^3He scattering. The points and squares are the experimental data,[42,43,45] and the triangles are from Ref. 44. The curves are the result of calculations using various potentials.

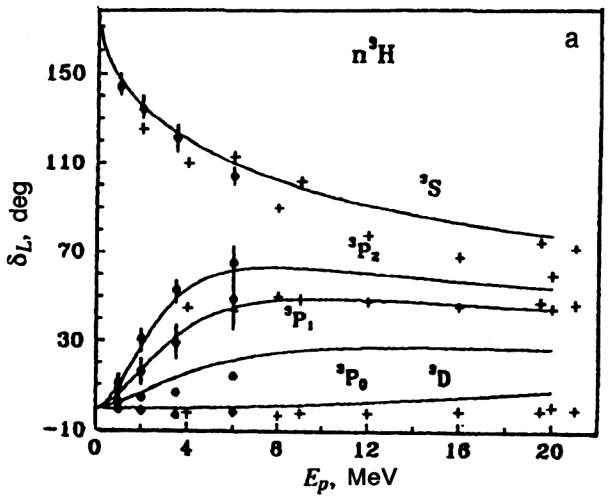

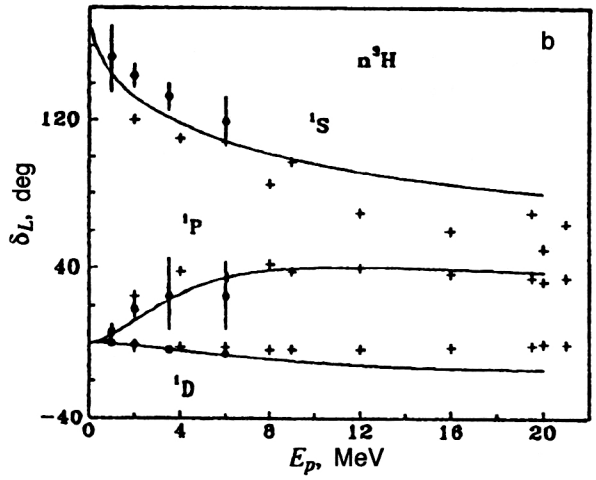

FIG. 10. Phase shifts of elastic n^3H scattering. The points are the experimental data,[47] the crosses are the RGM calculations from Ref. 48, and the solid lines are the results of calculations using the potentials of Table IV.

deformation, i.e., the assumption that the deuteron cluster inside the ^{3}He or ^{3}H nucleus cannot be associated with the properties of the free deuteron. This is completely reasonable from the viewpoint of the sizes of the deuteron and the ^{3}He and ^{3}H nuclei, because the deuteron radius is much larger than the radii of these nuclei. To obtain the correct radii and form factors of these nuclei it is necessary to compress the deuteron cluster by about 30–40% (Ref. 8). The asymptotic constant for this potential is 2.3(1) in both channels. When deformations are neglected, the radii are R_f=2.05 F and R_r=2.20 F in p^2H and R_f=1.95 F and R_r=2.12 F in n^2H. In Fig. 12 the solid line shows the momentum distributions of clusters in the ^{3}He nucleus obtained with the first set of parameters of the ground-state potential. The dashed line shows the results for the second potential. The experimental data are taken from Ref. 51.

3.4. The ^{2}H^{3}He cluster system

Let us now turn to the ^{2}H^{3}He system. In the doublet channel the phase shifts depend on the two orbital schemes {41} and {32}, as seen from Table I. In the quartet channel only the {32} scheme is allowed, and the states are pure.

Experimental data on the phase shifts are available only in a narrow energy range 0–5 MeV (Ref. 52). Therefore, to obtain the potential it is necessary to use the RGM calculations of the phase shifts from Ref. 53. The phase shifts calculated using the potentials of Table V are shown in Fig. 13 by the solid lines. Here the points and squares are the experimental P- and S-wave phase shifts from Ref. 52, and the crosses and circles are variants of the RGM calculations from Ref. 53. In Fig. 13a the dashed line shows the D-wave phase shifts of the potential from Ref. 6 with the parameters V_0=50 MeV and α=0.15 F^{-2}, which lead to a more correct description of the RGM D-wave phase shifts and roughly the same results for the S-wave phase shifts. In Table V we give the energies of the forbidden states for quartet potentials with the scheme {5} for L=0 and with the scheme {41} for L=1. The allowed states with {32} symmetry turn out to be unbound.

We see from Fig. 13b that the RGM and the experimental doublet S-wave phase shifts differ considerably from each other. The interaction parameters quoted in Table V were obtained from the experimental data, and the S-wave phase shift is shown by the dotted line. The description of the

TABLE V. Interaction potentials of p^2H and ^{2}H^{3}He cluster systems with mixed Young schemes in doublet channels. For all cases R_c=0. E_{bs} are the bound-state energies. The values of the energy for the n^2H and ^{2}H^{3}H systems are given in parentheses.

System	L_J	V_0 (MeV)	α (F^{-2})	V_1 (MeV)	β (F^{-1})	E_{bs} (MeV)
	S=1/2					
	Even	35.0	0.1			−9.3(−10.1)
p^2H		55.0	0.2			−11.4(−12.3)
	Odd	−0.4	0.01			
		10.0	0.16	0.6	0.1	
	S=3/2					
	Even	41.9	0.13	13.7	0.36	−4.2(−4.9)
	Odd	7	0.05			
	S=1/2					
	Even	45.5	0.15			−15.9(−17.0)
^{2}H^{3}He	Odd	44	0.1			−7.5(−8.1)
	S=3/2					
	Even	34.5	0.1			−12.9(−13.8)
	Odd	29	0.1			−1.3(−1.8)

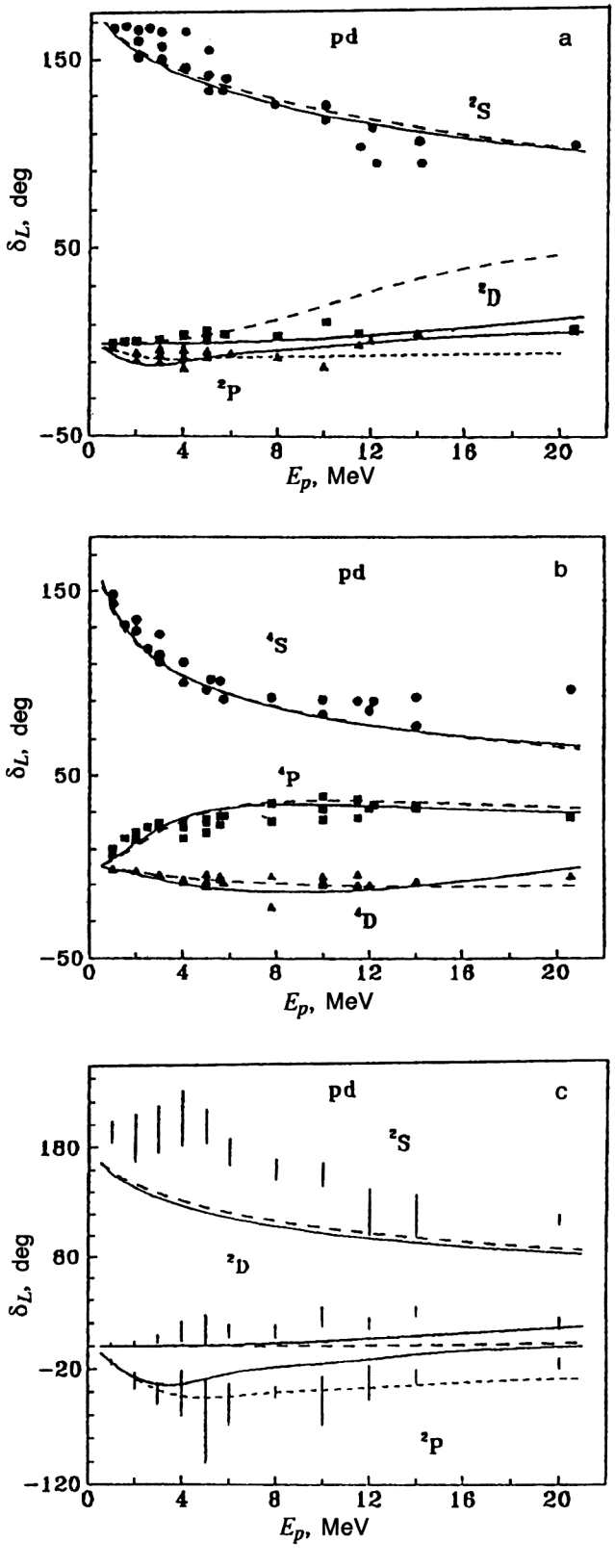

FIG. 11. Phase shifts of elastic p^2H scattering. The points, triangles, and squares are the experimental data,[49] the curves are the results of calculations using the potentials with the parameters in Table V, and in (c) the vertical lines are the error bars for pure phase shifts with scheme {3}, and the curves are the calculations for various potentials.

RGM S-wave phase shifts requires a potential with parameters $V_0=25$ MeV and $\alpha=0.15$ F^{-2}. The S- and D-wave phase shifts for this potential are shown by the solid lines. The doublet P-wave potential was obtained from RGM calculations and on the whole agrees with experiment. The cross sections for elastic scattering at 4.19 and 10 MeV calculated with these interactions agree with the experimental results of Refs. 20 and 54. We see from Table V that the P-wave state allowed in the doublet channel has energy inconsistent with the average energy of the P-wave bound state, because the potential depends on two orbital schemes.

Equation (20) was used to obtain the pure phase shifts in the doublet channel. These are shown by the vertical lines in Fig. 14. The parameters of the pure potentials are given in Table VI, and in the figure the solid lines show the phase shifts calculated with these potentials for the S, D, and $P_{3/2}$ waves. The dashed lines show the phase shifts for the potentials from Ref. 6 with the parameters $V_0=57$ MeV, $\alpha=0.16$ F^{-2}, $V_1=8.4$ MeV, and $\beta=0.21$ F^{-1} for even waves, and $V_0=69$ MeV and $\alpha=0.14$ F^{-2} for odd waves. The pure potentials with {41} symmetry give the correct energy of the P-wave levels of the ^{5}Li nucleus, and in the S-wave state there is a forbidden state with the {5} scheme.

3.5. The ^{2}H^{2}H cluster system

In scattering in the ^{2}H^{2}H system, the {22} orbital scheme is allowed in the channel with $S=2$, and the {31} scheme is allowed in the triplet channel. The singlet channel is compatible with the two symmetries {4} and {22}, as seen from Table I. Experimental data on the phase shifts in the ^{2}H^{2}H system are avaliable only in the range 8–12 MeV (Ref. 55). It is therefore necessary to use the results of the RGM calculations of the phase shifts.[56] In Figs. 15 and 16a the crosses show the RGM phase shifts, and the circles show the results of the phase-shift analysis. We see from Fig. 15a that there is a great difference between the various RGM calculations in the S wave of the singlet channel. The lower results were obtained using the multichannel version of the RGM, and the upper ones with the one-channel version. The triplet P-wave phase shifts also differ noticeably in these variants of the RGM calculation and lie somewhat lower than the experimental data. However, all the D- and S-wave phase shifts at $S=2$ are similar to each other and on the whole are consistent with the phase-shift analysis.

The triplet potential of the ^{2}H^{2}H system was constructed from the experimental data,[55] and the interactions with $L=0$ and 2 were constructed from the experimental data and the RGM calculations. The calculated phase shifts are shown by the solid lines in the figures. The potential parameters are given in Table VII. Two variants of the interaction are obtained in the singlet channel. The first contains a single bound state and describes the multichannel results, as shown by the dashed line in Fig. 15a. The second, which correctly reproduces the D-wave phase shift, leads to a compromise between the various RGM calculations.

Since for $S=0$ two schemes compatible with $L=0$ are allowed, while the {22} scheme also admits $L=2$, the second variant of the singlet interaction appears more realistic, as it

TABLE VI. p^2H and ^{3}He^{2}H interaction potentials in doublet channels with pure Young schemes. $R_c=0$ for all cases. E_{bs} are the bound-state energies. The energies for the n^2H and ^{2}H^{3}H systems are given in parentheses.

System	L_J	V_0 (MeV)	α (F^{-2})	V_1 (MeV)	β (F^{-1})	E_{bs} (MeV)
	Even	34.75	0.15			−5.49(−6.25)
p^2H		54.3	0.3			−5.49(−6.40)
	Odd	−2.4	0.01			
	Even	40.0	0.15	8.0	0.2	−7.1(−8.0)
^{2}H^{3}He	$P_{3/2}$	75.5	0.15			−16.4(−17.2)
	$P_{1/2}$	60.2	0.15			−8.9(−9.6)

has two deep bound levels in the S wave and one in the D wave. The latter is located at energy −13.3 MeV. The triplet potential has an allowed state consistent with the 2^- level at 22.1 MeV. The potential for $S=2$ contains a forbidden state with the {4} scheme.

Pure phase shifts of the singlet channel were obtained using Eq. (20) for $\{f_1\}=\{4\}$ and $\{f_2\}=\{22\}$. When only the results of the multichannel RGM are used, pure phase shifts are clearly obtained; they are shown by the points in Fig. 16b. When the results of both RGM variants are used, bands of values are obtained for the pure phases; these are shown by the vertical lines in the figure. The parameters of the pure potentials are given in Table VII. The S-wave potential correctly reproduces the locations of the bound states at energies −28.848 MeV and −3.748 MeV relative to the threshold of the cluster channel. The interaction parameters are uniquely fixed from the energies of these levels. However, although this potential describes the S-wave phase shift, it leads to a D-wave phase shift beginning at 180° and contains an unobserved state in the bound-state spectrum at −1.5 MeV. These results are shown by the solid lines in Fig. 16b. Therefore, for the D wave it is necessary to use a potential with different parameters which does not give bound states, but describes the phase shift, as shown by the dotted line in Fig. 16b. The pure S-wave potential in the ^{2}H^{2}H system leads to the correct radius of 1.64 F only when the deuteron is deformed by about 40%, just as for the p^2H channel of the ^{3}He nucleus. The asymptotic constant is 13.7(1.3); this is considerably larger than the experimental data,[27] which give values in the range 6–9.

3.6. The p^3H and n^3He cluster systems

The p^3H and n^3He systems are mixed in isospin, because for $T_3=0$ the values $T=0$, 1 are possible. Here both

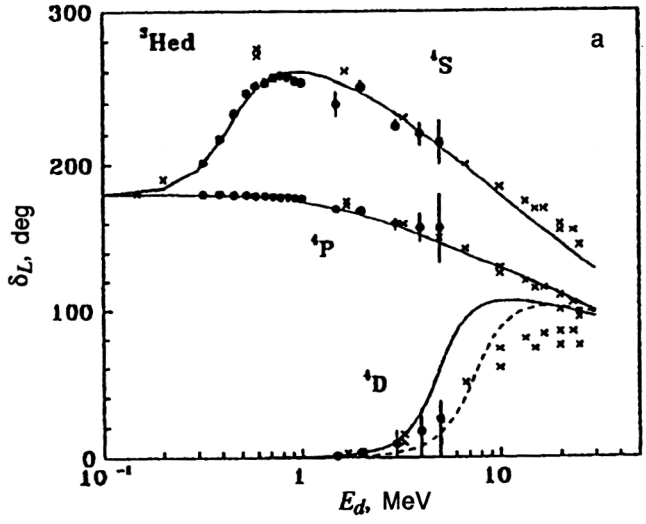

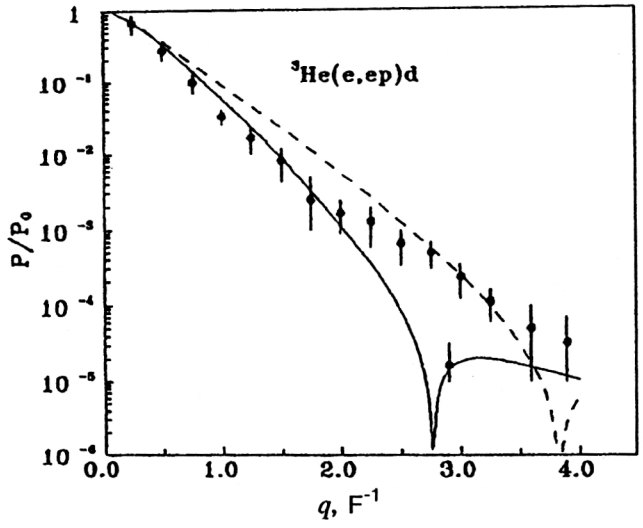

FIG. 12. Momentum distributions of p^2H clusters in the ^{3}He nucleus. The points are from experiment,[51] and the curves were calculated using the ground-state potentials in Table VI.

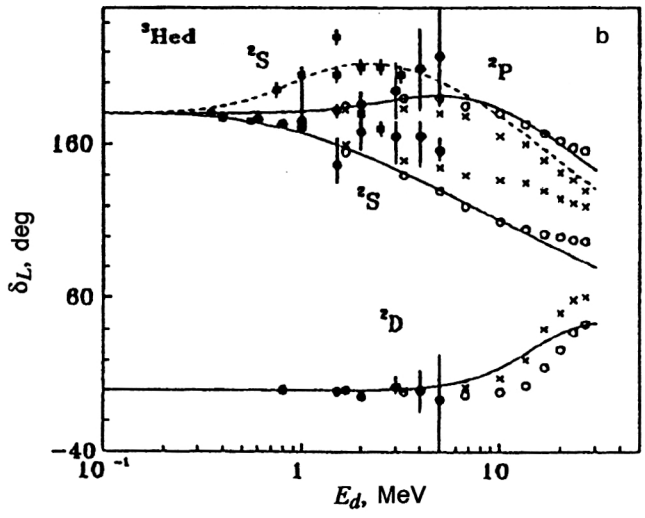

FIG. 13. Phase shifts of elastic ^{2}H^{3}He scattering. The points and squares are the experimental data,[52] the crosses and circles are different variants of the RGM calculations,[53] and the curves are calculated for various potentials.

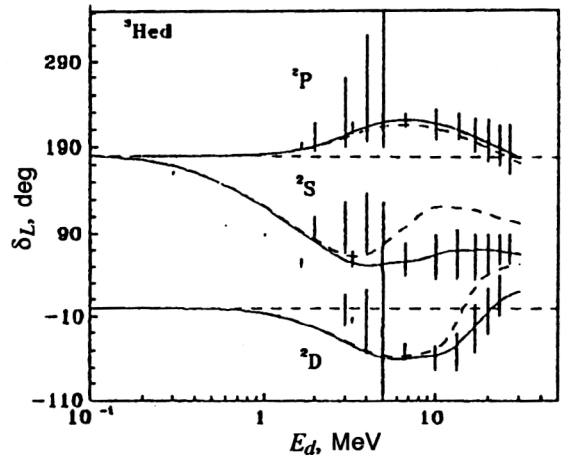

FIG. 14. The vertical lines are the error bars for pure $^2H^3He$ phase shifts with the scheme {41}, and the curves are calculated for various potentials.

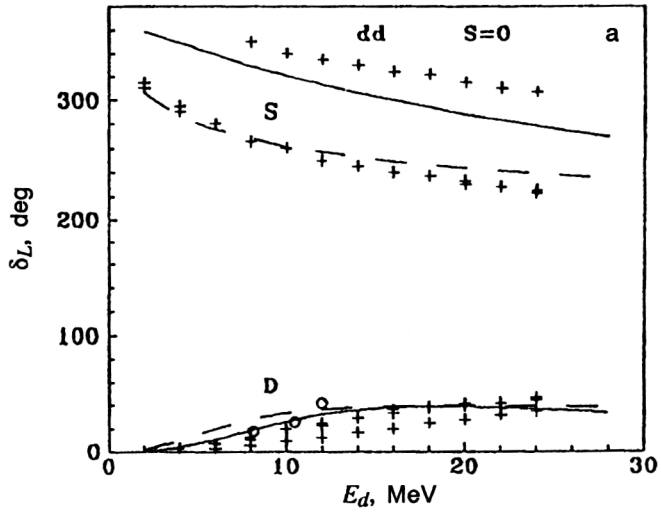

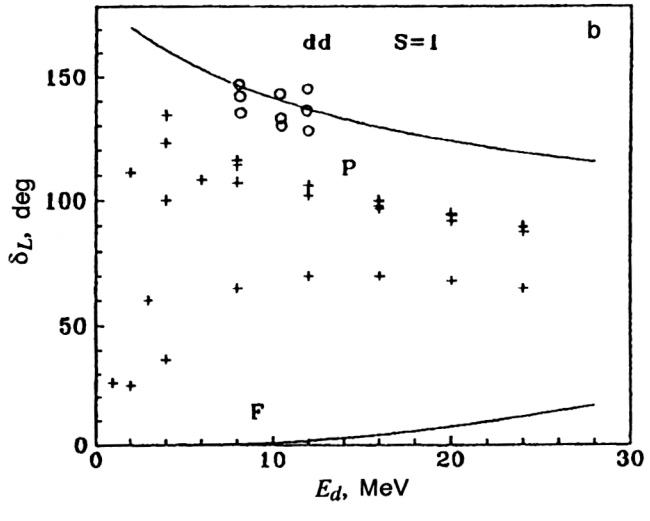

FIG. 15. Phase shifts of elastic $^2H^2H$ scattering. The circles are the experimental data,[55] the crosses are different variants of the RGM calculations,[56] and the curves are calculated for various potentials.

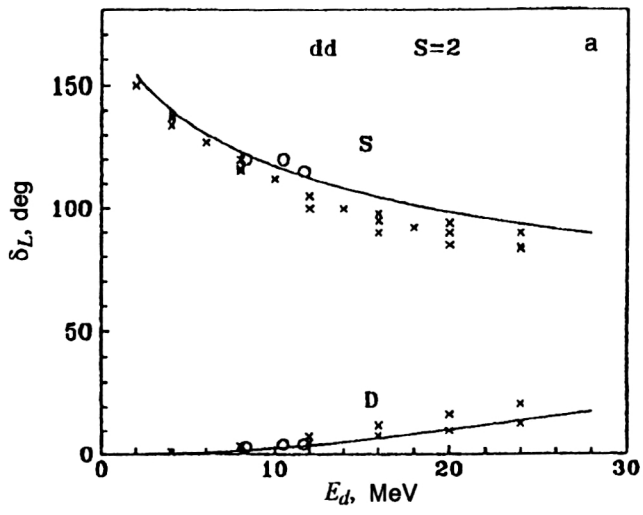

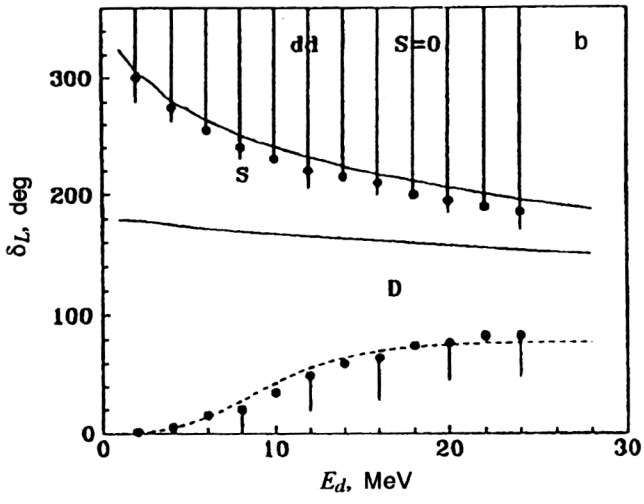

FIG. 16. (a) Phase shifts of elastic $^2H^2H$ scattering. The circles are the experimental data,[55] the crosses are different variants of the RGM calculations,[56] and the curves are calculated for various potentials. (b) The vertical lines are the error bars for pure phase shifts with the scheme {4}, and the curves are calculated using the potentials of Table VII.

the triplet and singlet phase shifts, and therefore the potentials, effectively depend on two values of the isospin. The isospin mixing leads to mixing in the Young schemes. In particular, in the singlet state the two orbital schemes {31} and {4} are allowed, as seen from Table I. Therefore, to obtain pure phase shifts with $T=0$, according to (20) it is necessary to use phase shifts which are pure in the isospin of the p^3He system with $T=1$. Only the {31} scheme is possible in the triplet state, but it is also mixed in isospin.[7,8]

There is a relatively large amount of experimental data on the p^3H phase shifts.[57,58] Two sets of phase shifts which reproduce the scattering cross sections are given in Ref. 58. The first agrees on the whole with the data of Ref. 57. In Figs. 17 and 18a we show the experimental isospin-mixed phase shifts and the calculated phase shifts of p^3H elastic scattering. The potential parameters are given in Table VIII. Since the potentials are mixed, the energy of the singlet S-wave interaction does not correspond to the experimental binding energy of the ^{4}He nucleus. In the triplet S-wave state

TABLE VII. Interaction potentials in the $^2H^2H$ system which are mixed in the singlet channel and pure with {4} symmetry. $R_c=0$ for all cases. E_{bs} are the bound-state energies.

S, L_J	V_0 (MeV)	α (F^2)	E_{bs} (MeV)
$S=0$	9.0	0.05	−1.5
	108.0	0.125	−17.1; −61.5
$S=1$	51	0.16	−2.0
$S=2$	40	0.24	−6.9
^1S {4}	47.15	0.073	−23.85; −3.73
^1D {4}	35.0	0.11	

there is a forbidden state with the {4} scheme. The states with {31} symmetry allowed in the two channels have a single quantum, and the P-wave potentials do not contain bound states.

After using (20) to find the pure phase shifts with {4} symmetry, which are shown by the points in Fig. 18b, these phase shifts are used to find the pure interaction potentials with the parameters given in Table IX, where we also give the bound-state energies. The calculated pure phase shifts for these potentials at $S=0$ are shown by the solid lines in Fig. 18b, and the calculated characteristics of the ^{4}He nucleus in the p^3H and n^3He models are given in Table X (Ref. 8) along with the experimental data of Refs. 25 and 27.

4. PHOTOPROCESSES ON LIGHT NUCLEI

4.1. Photoprocesses on ^{6}Li and ^{7}Li

The total cross sections for photoprocesses have been calculated earlier using a phenomenological potential model[59] similar to the one used here and the resonating-group method[30,60,61] for the ^{4}He^{2}H, ^{4}He^{3}H, and ^{4}He^{3}He systems. The total cross sections in the ^{4}He^{2}H channel of the ^{6}Li nucleus have been calculated for interactions with forbidden states using the three-body ground-state wave functions.[62] The total cross sections have been calculated in the two-cluster model with forbidden states using Gaussian potentials consistent with the elastic scattering phase shifts.[10]

Turning to the cross sections for photoprocesses, we note that the spin electric operator $Q_{Jm}(S)$ in (2) gives a relatively small contribution to the total cross section for a process. We can therefore consider only the first operator for EJ transitions. However, for example, for $E1$ processes in the ^{4}He^{2}H system the spin term can give a noticeable contribution, owing to the smallness of the cross section due to the orbital operator, because in nuclei with $N=Z$ the $E1$ transitions with $\Delta T=0$ are strongly suppressed. In the cluster model this fact is reflected in the factor $(Z_1/M_1-Z_2/M_2)^2$, which is equal to zero under these conditions. An $E1$ transition due to the orbital operator can arise in such nuclei only if the condition $M=2Z$ is not exact. For example, in the ^{4}He^{2}H system of the ^{6}Li nucleus, the masses of the deuteron and ^{4}He are not integers, but are $M_d=2.0135537$ and $M_\alpha=4.0015061$.

The $E1$, $E2$, and $M1$ transitions and the contribution of the spin part of the electric operator were included in the calculation of the cross sections in the ^{4}He^{3}H and ^{4}He^{3}He systems. Let us consider, for example, the $E1$ transition,

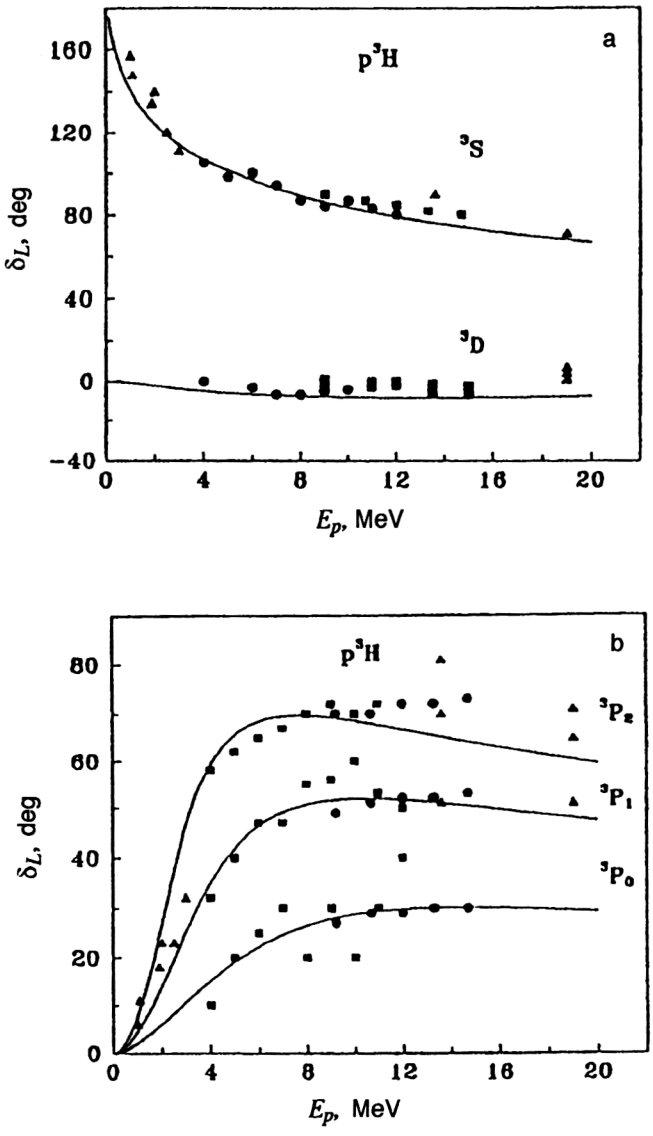

FIG. 17. Phase shifts of elastic p^3H scattering. The circles, triangles, and squares are the experimental data,[57,58] and the curves are calculated using the potentials of Table VIII.

when the capture can occur both on the ground bound state with $J=\frac{3}{2}^-$ and energy −2.47 MeV in ^{7}Li and −1.59 MeV in ^{7}Be and on the first excited state with $J=\frac{1}{2}^-$ and energy −1.99 MeV and −1.16 MeV, respectively. The ground-state capture occurs from the S, $D_{3/2}$, and $D_{5/2}$ scattering states on the first excited S and $D_{3/2}$ state. The potential parameters used in the calculations are given in Table II.

The calculated cross sections for EJ and $M1$ capture of ^{4}He^{3}H and ^{4}He^{3}He are shown in Fig. 19. The experimental results[63,64] and the $E1$ calculations from Ref. 63 (upper dotted line in Fig. 19a) are also shown. The dot–dash line in Fig. 19b shows the RGM calculations for the $E1$ transition.[12,30,60,61] We see from these figures that the cross sections for $E2$ and $M1$ processes are one and a half and three orders of magnitude lower than the $E1$ cross section and do not contribute significantly to the total cross sections. The peak in the $E2$ cross section for ^{4}He^{3}H capture corresponds to the resonance in the $F_{7/2}$ phase shift at energy 2.16

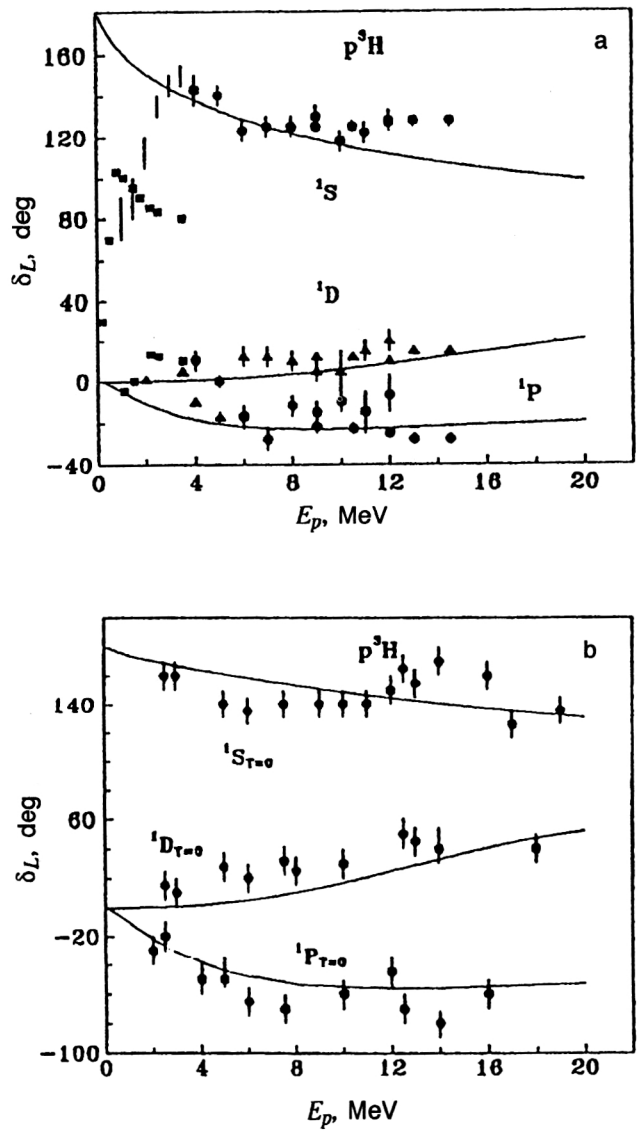

FIG. 18. (a) Phase shifts of elastic p^3H scattering. The circles, triangles, and squares are the experimental data,[57,58] and the curves are calculated for various potentials. (b) The points are the pure phase shifts with scheme {4}, and the curves are the calculated pure phase shifts for potentials with the parameters from Table VIII.

MeV in the c.m. frame. A similar peak is also observed in the cross section for ^{4}He^{3}He capture at 7.0 MeV, which corresponds to a resonance at 2.98 MeV (c.m. frame) relative to the cluster thresholds. The calculated $M1$ cross sections are in good agreement with the RGM results.[61] In Fig. 19a the dot–dash line labeled $E1'$ shows the cross section due to the spin term $Q_{Jm}(S)$ of the electric $E1$ operator, which in the ^{4}He^{3}H system is considerably smaller than the orbital term $Q_{Jm}(L)$, and its contribution to the total $E1$ cross section can actually be neglected. In all the calculations the cluster magnetic moments were taken to be $\mu_t = 2.9786\mu_0$ and $\mu_{He} = -2.1274\mu_0$.

The S factor was also calculated for ^{4}He^{3}H capture. At 20 keV it is 0.087 keV·b, to be compared with the value 0.064(16) keV·b quoted in Refs. 63 and 64. Other experimental data give 0.134(20) (Ref. 65). In ^{4}He^{3}He capture the S factor at 40 keV is 0.47 keV·b, in good agreement with the data,[63,66] which give a value in the range 0.47–0.63 keV·b. A value in the range from 0.5 to 0.6 keV·b is usually obtained in RGM calculations.[12,60] In the potential approach[13,31,67] the calculations give 0.47(2) keV·b, and the value 0.56 keV·b was obtained in Ref. 59. There are two sets of experimental data on the S factors for this system.[63] One of them leads to the value $S(0) = 0.3(3)$ keV·b, which differs from $S(0) = 0.61(7)$ keV·b. The average value of 0.45 keV·b agrees well with the above value. In Fig. 20 we show the astrophysical S factors for ^{4}He^{3}H and ^{4}He^{3}He capture for energies up to 3 MeV obtained using the $E1$ cross sections and compare them with the RGM calculations[12,30,60] (dashed lines). The experiment is described in Refs. 63 and 64.

The value of P_J for the ^{4}He^{2}H system in the case of $E2$ transitions can be written as

$$P_J^2 = 2J_i + 1, \tag{21}$$

if the capture occurs on the ground state from scattering states with $L=2$ and $J_i = 1, 2, 3$. The potential parameters used in the calculations are given in Table II.

The cross section for $E2$ capture, which is shown by the solid line in Fig. 21 along with the experimental data,[68] has a peak at 0.71 MeV and also a second maximum at about 2.5–3 MeV, which corresponds to a resonance in the D_2 wave with energy 2.84 MeV. The lower dotted line shows the cross sections for $M2$ capture from the P_1 and P_2 scattering states on the ground state. The upper dotted line shows the calculated $E2$ cross sections from Ref. 59.

We also calculated the cross section for $E1$ capture on the ground state from the continuum with $J_i = 0$, 1, 2 and $L=1$ for the orbital ($E1$) and spin ($E1'$) terms separately and the total of these cross sections including interference (see the lower solid line in Fig. 21). It is noticeably smaller

TABLE VIII. Interaction potentials in the p^3H system with mixed Young schemes. $R_c = 0$ for all cases. E_{bs} are the bound-state energies. The energies for the n^3He system are given in parentheses.

L_J	V_0 (MeV)	α (F^{-2})	V_1 (MeV)	β (F^{-1})	E_{bs} (MeV)
$S=0$					
Even	50	0.2			−10.4(−11.4)
Odd	−3	0.03			
$S=1$					
Even	55	0.39	6.0	0.39	−1.2(−2.0)
P_0	11	0.1			
P_1	17.5	0.1			
P_2	22	0.1			

TABLE IX. Interaction potentials of the p^3H cluster system with pure Young schemes. $R_c=0$ for all cases. The energies for the n^3He system are given in parentheses.

L_J	V_0 (MeV)	α (F^{-2})	V_1 (MeV)	β (F^{-1})	E_{bs} (MeV)
$S=0$					
Even	63.1	0.17			−19.82
Odd	−8	0.03			
$S=1$					
Even	70.0	0.39	15	0.39	−1.4(−2.4)
P_0	11	0.1			
P_1	19	0.1			
P_2	24	0.1			

than the $E2$ cross section and practically does not contribute to the total cross sections at energies above 0.5 MeV. In Fig. 22a the solid line shows the cross sections for photodisintegration of ^{6}Li in the ^{4}He^{2}H channel together with the experimental results[68,69] and the calculations (dashed line) of Ref. 62 using the ground-state three-body wave functions. In Fig. 22b we give the S factors obtained from the $E1$ and $E2$ cross sections. We clearly see that at low energies the $E1$ cross section dominates. Linear extrapolation of the S factors to zero gives $S(E2)=3\times10^{-7}$ keV·b and $S(E1)=1.2\times10^{-6}$ keV·b, so that the overall S factor is 1.5×10^{-6} keV·b. This result is in good agreement with the calculations of Ref. 70.

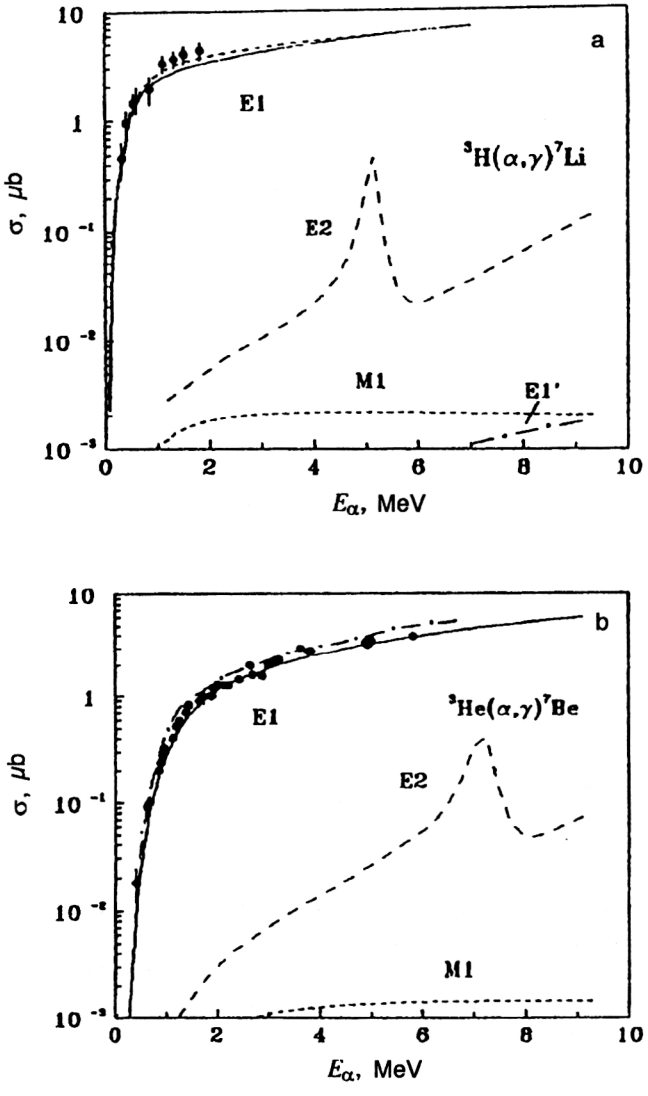

FIG. 19. Total cross sections for radiative capture in the ^{4}He^{3}H and ^{4}He^{3}He systems with production of ^{7}Li and ^{7}Be nuclei in the ground and first excited states. The curves are the cross sections calculated for various transitions (see explanation in the text). The points are the experimental data from Refs. 63 and 64.

In the case of $E1$ capture of ^{3}He^{3}H on the ground state of ^{6}Li, P_J is written as (21) for initial states with $J_i=0$, 1, 2 and $L=1$. The $E1$ transition to the 3^+ resonance state can also be studied in the ^{3}He^{3}H model. The parameters of the ^{3}He^{3}H potentials taking into account spin–orbit splitting are given in Table II. The calculated total capture cross section with S-wave potential correctly reproducing the nuclear binding energy in this channel is shown by the solid line in Fig. 23. The experimental data are taken from Ref. 71. We see that the use of this potential and the P-wave interaction reproducing the energy behavior of the phase shifts gives agreement with these experimental data. There are also other measurements of the cross sections[72,73] which differ significantly from those given in the figure.

For $M1$ transitions to the ground state we studied the process in which the spin state changes from singlet to triplet. Only the spin term $W_{Jm}(S)$ remains in the transition operator. The quantity P_J is given by (21) for $E2$ transitions to the ground state from states with $L=2$ and $J_i=1$, 2, 3. The results of these calculations are shown by the dotted and dashed lines in Fig. 23. In Fig. 24a we give the S factor for ^{3}He^{3}H capture at low energies. Linear extrapolation gives 0.06 keV·b for the S factor at zero energy in the $E1$ process. In Fig. 24b we show the calculated cross sections for capture on the 3^+ level for the potentials of Table II together with the data and calculations (dotted line) from Ref. 74. Here as the D_3 potential we used interactions with depth 105 MeV

TABLE X. Characteristics of the ^{4}He ground state in n^3He and p^3H cluster models.

Channel	E (MeV)	C_0	R_r	R_f
p^3H calculation	−19.822	4.5(1)	1.761	1.693
Experiment	−19.815	5.2(1);4.2(2)		1.673(1)
n^3He calculation	−20.861	4.4(1)	1.838	1.699
Experiment	−20.578	5.1(4)		1.673(1)

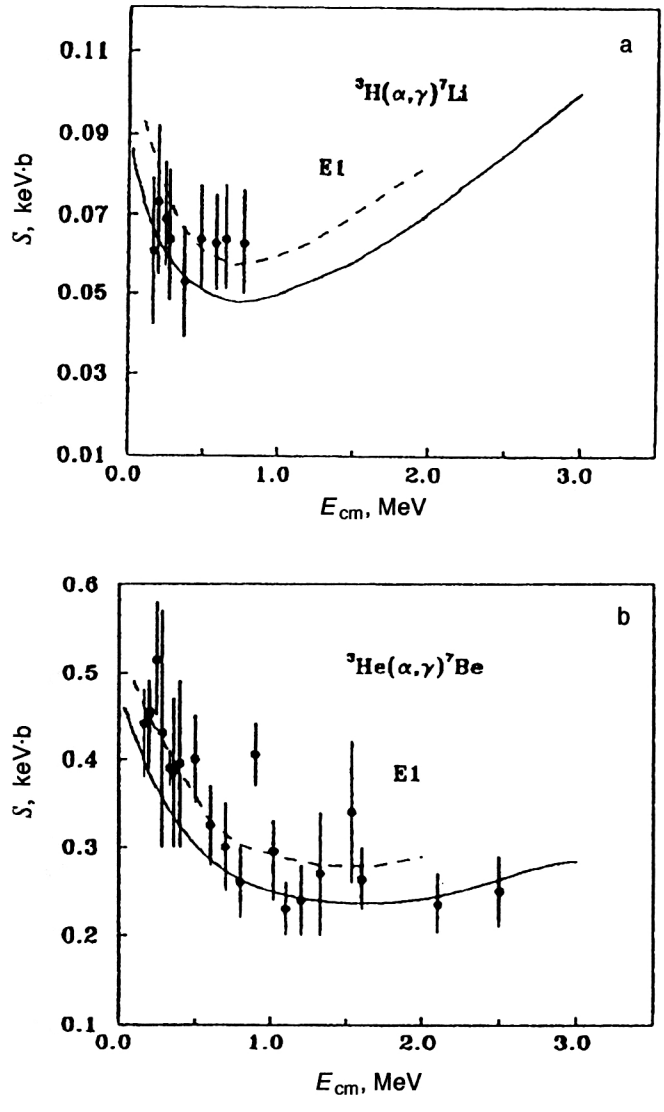

FIG. 20. Astrophysical S factors at low energies for ^{4}He^{3}H and ^{4}He^{3}He capture. The points are the experimental data from Refs. 63 and 64. The solid lines were calculated for the potentials of Table II, and the dashed lines are the RGM calculations from Refs. 60 and 61.

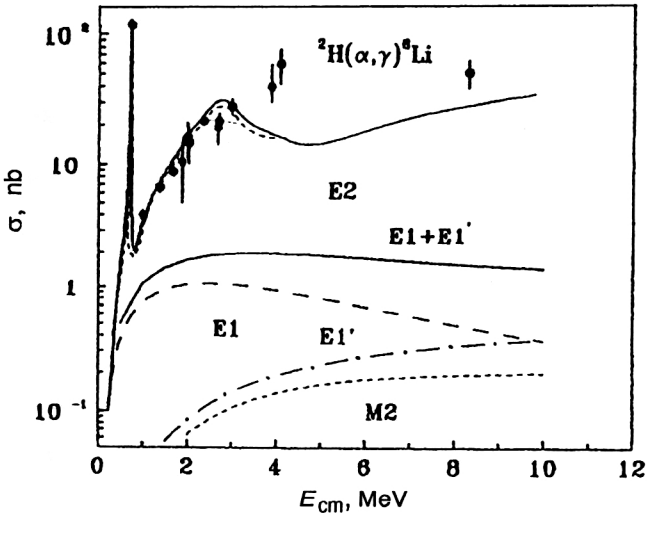

FIG. 21. Total cross sections for radiative capture in the ^{4}He^{2}H system with production of the ^{6}Li nucleus in the ground state. The curves are the cross sections calculated for various processes (explained in the text). The points are the experimental data from Ref. 68.

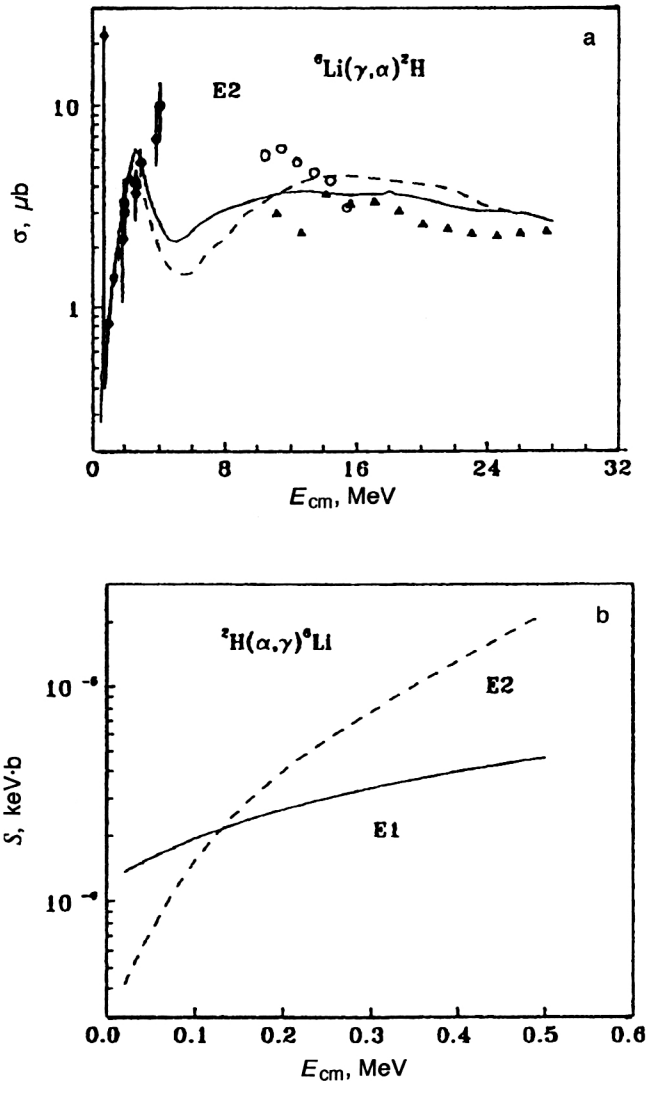

FIG. 22. (a) Total cross sections for photodisintegration of the ^{6}Li nucleus in the ^{4}He^{2}H channel. The solid line is the $E2$ cross section calculated for the potentials of Table II, and the dashed line is the cross section calculated in Ref. 62 with ground-state three-body wave functions. The points are the experimental data.[68,69] (b) Astrophysical S factors for $E1$ and $E2$ processes.

(solid line) and 107.5 MeV (dashed line), with $\alpha=0.18$ F^{-2} in both cases.

4.2. Photoprocesses for the ^{3}He, ^{3}H, and ^{5}Li nuclei

The differential cross sections for photoprocesses in the N^{2}H, N^{3}H, and ^{2}H^{3}He systems for potentials containing forbidden states and separated on the bases of orbital schemes have been successfully calculated earlier in Ref. 6. In Ref. 75 we studied the total cross sections for such systems using cluster models with forbidden states and separation on the basis of the Young schemes.

The $E1$ and $E2$ transitions due to the orbital part of the electric operator $Q_{Jm}(L)$ were taken into account in the calculation of the total cross sections. The magnetic cross sections and spin-dependent parts of the electric operator turned out to be relatively small. In the N^{2}H system $E1$ transitions are possible between the ground pure ^2S state and the ^2P

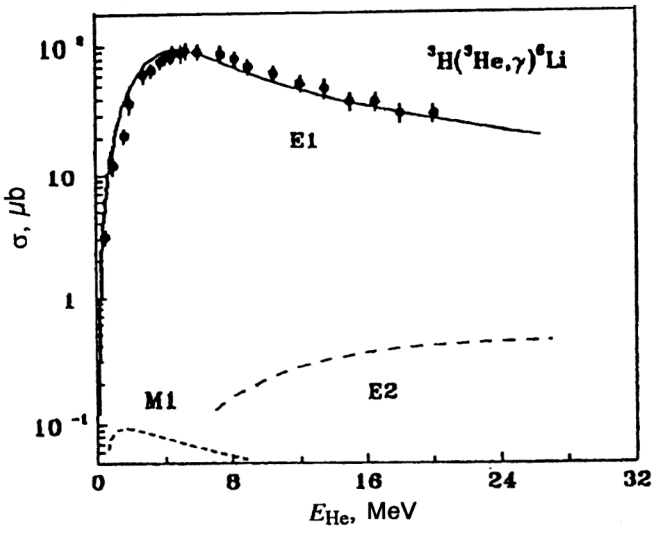

FIG. 23. Total cross sections for radiative capture in the ^{3}He^{3}H channel with production of the ^{6}Li nucleus in the ground state. The solid line is the $E1$ cross section calculated for the potentials in Table II, the dotted line is the cross section for the $M1$ process, and the dashed line is the $E2$ cross section. The points are the experimental data of Ref. 71.

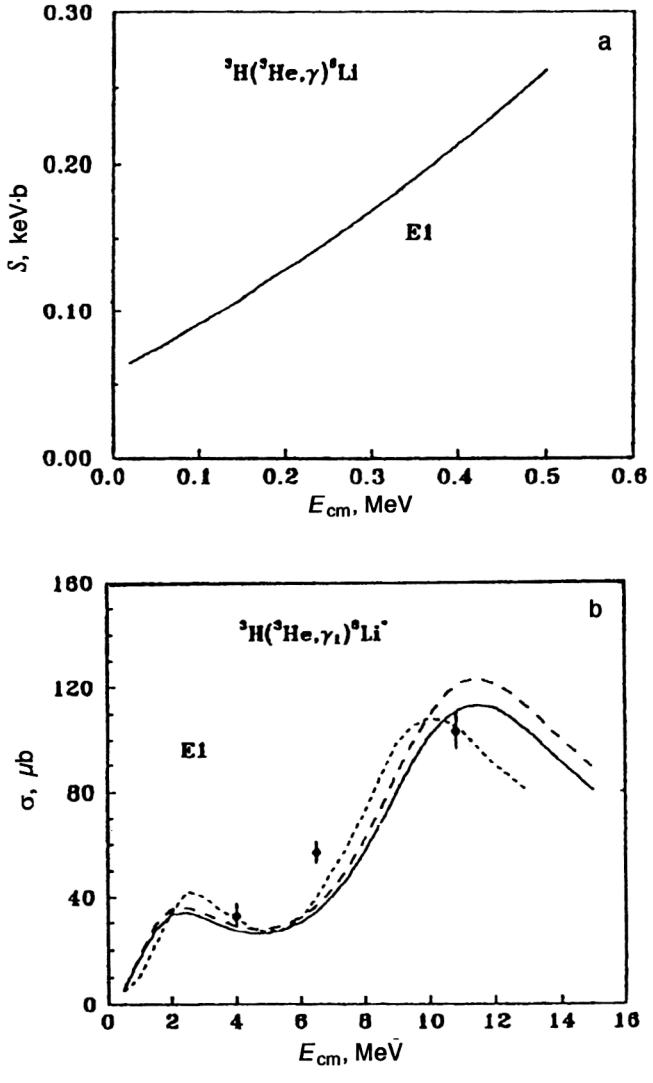

FIG. 24. (a) Astrophysical S factor for ^{3}He^{3}H capture. (b) Total cross section for radiative capture in the ^{3}He^{3}H channel with production of the ^{6}Li nucleus in the resonance 3^+ state. The points are the experimental data from Ref. 74. The dotted line is the calculated cross section for $E1$ capture on the 3^+ level obtained in Ref. 74. The solid and dashed lines are the cross sections calculated for the potentials in Table II.

scattering state. The quantity P_J^2 in (5) for photodisintegration can be written as (21) if J_i is replaced by J_f, where J_f is the angular momentum of the final state and can take the values $\frac{1}{2}^-$ and $\frac{3}{2}^-$. In the case of $E2$ processes, transitions can occur between the pure ground state and the doublet D-wave scattering state. Again in this case P_J^2 is written as (21) with $J_f=\frac{3}{2}^+$ and $\frac{5}{2}^+$. The cross sections for photoprocesses are proportional to the factor $(Z_1/M_1^J+(-1)^J Z_2/M_2^J)^2$, which has the same value in the n^2H and p^2H systems in the case of $E1$ transitions and values differing by about an order of magnitude for $E2$ transitions. Therefore, the $E2$ cross section is significant only in the p^2H system. However, this does not explain the difference in the values of the experimental cross sections for p^2H and n^2H photodisintegration.

In Fig. 25 the solid lines show the calculated total cross sections for photodisintegration of the ^{3}H and ^{3}He nuclei in the n^2H and p^2H channels using the first variant of the ground-state potential and the P-wave interaction with peripheral repulsion (see Tables V and VI). The experiment was performed in Refs. 76 and 77. The dashed line shows the results obtained with the same ground-state potential, but with a purely repulsive version of the P-wave interaction. The use of the second version of the ground-state potential for any P-wave interaction leads to photodisintegration cross sections reaching only 600 mb at the maximum, as shown by the dotted lines in Fig. 25. The lower dashed line in Fig. 25b shows the cross section for the $E2$ process. In Fig. 26 we show the astrophysical S factor due to the $E1$ transition. The experimental data were obtained by rescaling the data of Ref. 78. The notation for the curves is the same as for photodisintegration. Linear extrapolation of the $S(E1)$ factor to zero energy gives $1.0(2)\times10^{-4}$ keV·b for the solid line and $1.6(2)\times10^{-4}$ keV·b for the dashed line.

There are quite a few calculations of the cross sections for these processes based on various model approaches. In particular, in some versions of the method of hyperspherical functions it is possible to reproduce the total cross sections at low energies.[77] However, in contrast to the approaches discussed above, in these approaches the supermultiplet symmetry of the wave function with separation on the basis of Young schemes, which makes it possible to analyze the structure of intercluster interactions and determine the presence and location of allowed and forbidden states, is usually not considered.

The quantity P_J^2 for $E1$ capture in the ^{2}H^{3}He system can be written as (21) with $J_f=\frac{1}{2}^-$, $\frac{3}{2}^-$ if capture occurs from the S wave to $^2P^{\{41\}}$ states of the final nucleus, which are not stable. The energy of the $P_{1/2}^{\{41\}}$ level is about 9 MeV, and the width is of order 5 MeV (Ref. 23). The value of P_J^2 is two times larger for capture from the ^2D wave than for capture

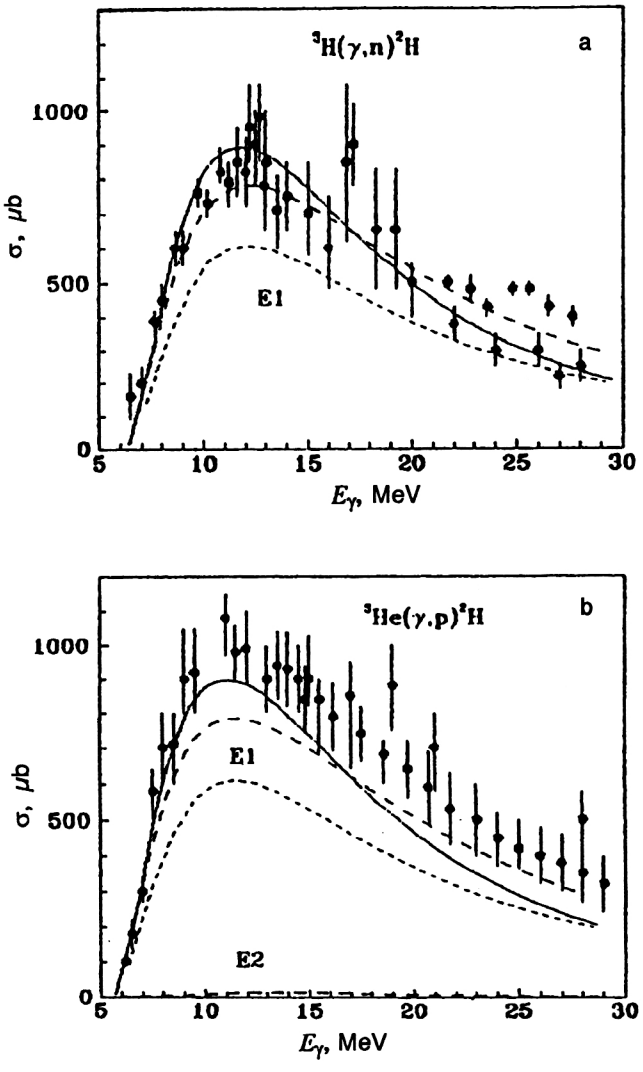

FIG. 25. Total cross sections for photodisintegration of ^{3}H nuclei in the n^2H channel and ^{3}He nuclei in the p^2H channel. The curves were calculated for the potentials in Tables V and VI. The experimental results are from Refs. 76 and 77.

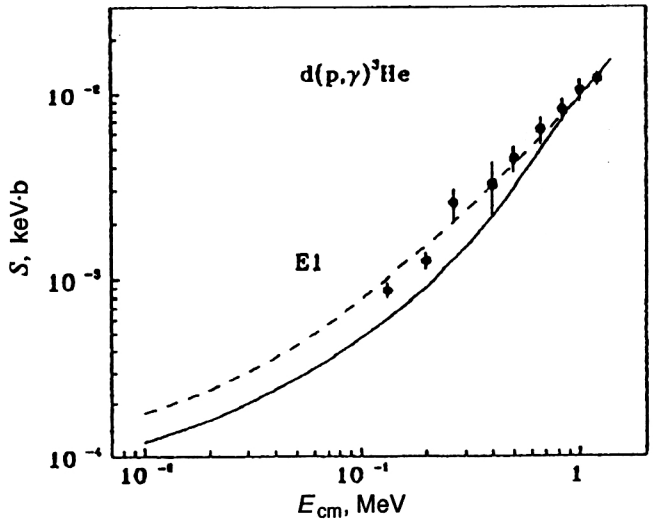

FIG. 26. Astrophysical S factor for p^2H capture. The curves were calculated for various potentials. The experimental results are from Ref. 78.

from the S wave if the spin–orbit splitting is not taken into account.

In Fig. 27a we show the calculated cross sections for $E1$ radiative capture in the ^{2}H^{3}He system in the energy range 10 keV–40 MeV. The dot–dash line shows the total summed cross section for $E1$ transitions from the S- and D-scattering waves to the $P_{3/2}$ level with the interaction from Table V for even waves used as the scattering potential. Its S-wave phase shift is shown by the dotted line in Fig. 13b and describes the experimental data. The solid line shows the $E1$ cross section for the S- and D-wave scattering potentials with the parameters $V_0=25$ MeV and $\alpha=0.15$ F^{-2} describing the RGM S-wave phase shift, as shown by the solid line in Fig. 13b. The dashed lines show the contributions from the S and D waves for transition to the $P_{3/2}$ level. The dotted line is the total cross section for the transition to the $P_{1/2}$ level. The two peaks observed in the cross sections for capture on both ^2P levels come from resonances in the ^2S and ^2D waves, respectively.

In Fig. 27b we show the astrophysical S factors for transitions to $P_{3/2}$ (solid line) and $P_{1/2}$ (dashed line) levels due to the $E1$ process. Linear extrapolation of the S factors to zero energy gives $S(3/2)=3(1)\times10^{-3}$ keV·b and $S(1/2)=7(1)\times10^{-4}$ keV·b. The S factor for the scattering potential describing the experimental S-wave phase shift is shown by the dot–dash line and at zero energy is $1.3(2)\times10^{-1}$ keV·b.

4.3. Photoprocesses in the ^{2}H^{2}H cluster channel of ^{4}He

Photodisintegration of the ^{4}He nucleus has been investigated in many studies,[79] but potentials containing forbidden states were not used. Such interactions were used in Ref. 6 to calculate the differential cross sections, and we studied the total cross sections in Ref. 80.

Since in the ^{2}H^{2}H system the main contribution comes from the $E2$ transition which can occur between the pure ground S state and the singlet D-wave scattering state, these two interactions can be improved. For the pure S-wave potential we shall use the set of parameters given in Table VII, which allows the bound-state energies to be reproduced exactly. For the singlet potential we shall study the two versions of the singlet interactions from Table VII. The first describes the S- and D-wave phase shifts, as shown in Fig. 15a, and does not contain any bound state in the D wave. The second describes the D-wave phase shift, has forbidden states, and can be used to make a compromise between the various S-wave phase shifts obtained by the RGM (see the solid line in Fig. 15a).

In calculating the total cross sections we considered only the $E2$ transition due to the orbital part of the electric operator $Q_{Jm}(L)$. The magnetic cross sections and spin-dependent parts of the electric operator turned out to be relatively small, and $E1$ processes are completely forbidden, owing to the presence of the cluster factor, which is equal to zero in the ^{2}H^{2}H system.

In Fig. 28a the solid line shows the calculated total cross sections for photodisintegration of the ^{4}He nucleus in the ^{2}H^{2}H channel for a deep singlet potential containing a bound

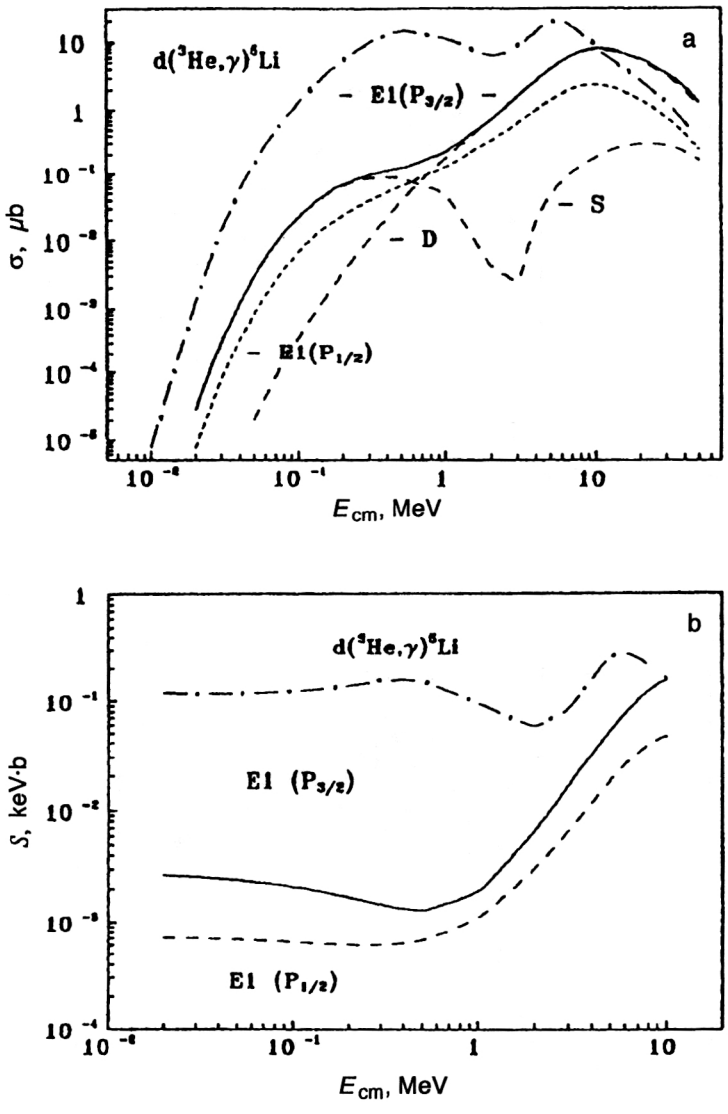

FIG. 27. (a) Total cross sections for ^{3}He^{2}H capture for ^{5}Li. (b) Astrophysical S factor for ^{3}He^{2}H capture calculated for various potentials.

state in the D wave. The experimental data obtained by rescaling the capture cross sections up to 10 MeV and from the cross sections for electrodisintegration at higher energies are from Refs. 81 and 82, respectively (the points and triangles in Fig. 28a). The circles show the results of the measurements made in Ref. 83. We see that the data agree well with each other only in the series of studies of Ref. 81, and these data also agree with the results of Ref. 83 at low energies. At higher energies the various measurements are contradictory. For example, there are indications of a second maximum at 20 MeV in Ref. 82, while in Ref. 83 the cross section clearly falls off at energies above 10 MeV.

The cross sections calculated using a shallow singlet D-wave interaction turn out to be an order of magnitude larger than the experimental ones. Any other set of parameters which allows description of the D-wave phase shift and produces bound states in the D wave gives calculated cross sections which are too large compared with experiment. And if we drop the requirement that the photodisintegration cross sections be described, we are forced to favor deep singlet interactions having bound states in the D wave. If for the pure ground-state potential we use the interaction with different parameters[82] which do not exactly reproduce the energies of the two bound states, the photodisintegration cross section is decreased by several times while the maximum is preserved at the same energies.

In Fig. 28b we show the calculated S factor of ^{2}H^{2}H capture at energies of 100 keV to 10 MeV (solid line) in comparison with the experimental data[81] and one version of the calculations performed in Ref. 79 (dashed line). We see that the calculated S factor describes the experimental data at energies of up to 1–2 MeV, and the shape is practically the same as in Ref. 79. At lower energies the cross section for $E2$ transitions of the type $^2S \rightarrow {}^2D$ turns out to be too small to explain the experimental data. At energies below 1 MeV the main contribution comes from the cross sections for the $E2$ process with transition from the quintet S wave to the D component of the ground-state wave function,[79] which is absent in the model used here.

4.4. Photoprocesses in the p^3H and n^3He cluster channels of the ^{4}He nucleus

The differential cross sections for the p^3H system using potentials with forbidden states and separation on the basis

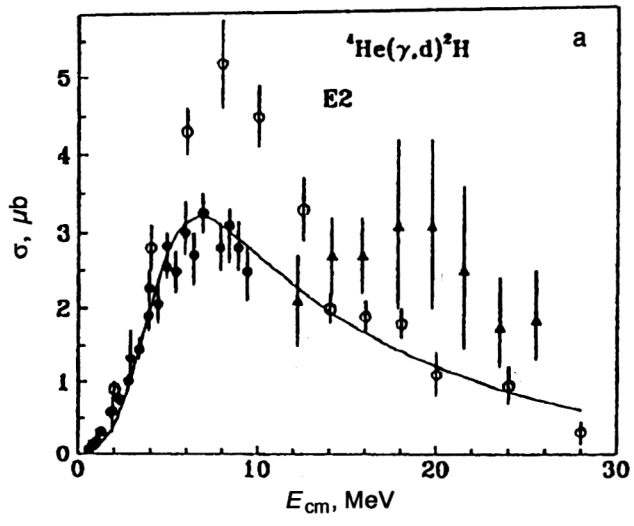

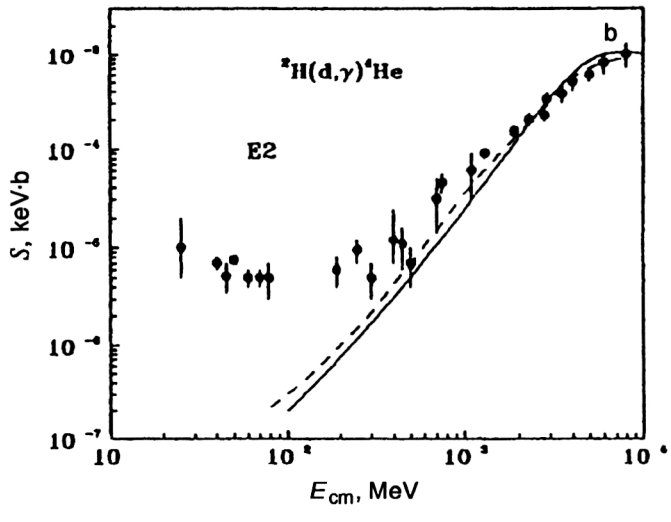

FIG. 28. (a) Total cross sections for photodisintegration of the ^{4}He nucleus in the ^{2}H^{2}H channel. The curve was calculated for the deep D potential of Table VII. The points, triangles, and circles are the experimental data from Refs. 81–83. (b) Astrophysical S factor for ^{2}H^{2}H capture. The solid line was calculated for the potentials of Table VII. The dashed line is the calculation from Ref. 79, and the points are the experimental results of Ref. 79.

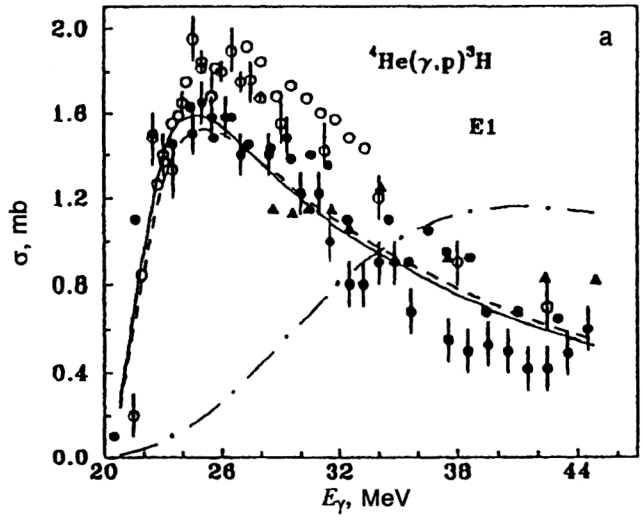

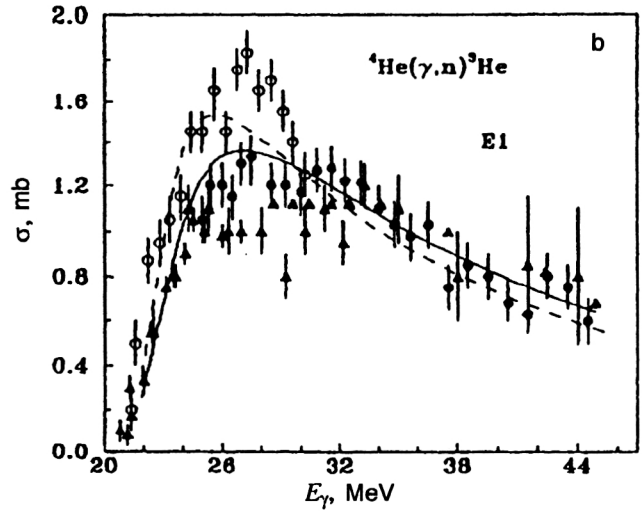

FIG. 29. Total cross sections for photodisintegration of the ^{4}He nucleus in the p^3H and n^3He channels. The curves were calculated for various potentials. The points, triangles, and circles are the experimental results from Refs. 86–91.

of Young schemes have been calculated earlier in Ref. 6. We calculated the total cross sections for these interactions in Ref. 84.

For $E1$ processes it is possible to have transitions between the pure ground state with $T=0$ and the singlet P-wave scattering state. If it is assumed that the main contribution to the cross sections comes from processes with change of isospin $\Delta T=1$ (Ref. 85), then it is necessary to use the P-wave potential from the $T=1$ isospin-pure singlet state of the p^3He system. In the case of transitions with $\Delta T=0$ we use the potential of the pure singlet P-wave phase shift with $T=0$ for the p^3H system. Three variants of the interaction are given in Ref. 84 for the $T=0$ ground state, but here we shall use only one of them. Its parameters are given in Table IX. The parameters of the P-wave interaction of p^3He are given in Table IV, and the phase shifts are shown in Figs. 8 and 9.

In Fig. 29a the dashed line shows the calculated total cross sections for photodisintegration of ^{4}He in the p^3H channel for transitions with $\Delta T=1$. The experimental results are taken from Refs. 86 and 87 (circles), Ref. 88 (triangles), and Ref. 89 (points). We see that the spread in the various data reaches 20–30%, with the later measurements[88,89] lying considerably lower than the earlier ones.[86,87] Since the P-wave potential was selected as a compromise between the various phase-shift analyses, its value is not determined uniquely. Therefore, it is possible to slightly increase its depth, taking $V_0=15$ MeV and $\alpha=0.1$ F^{-2}. Then at the maximum the cross section is increased by about 0.1 mb and agrees somewhat better with the experimental data,[88,89] as shown by the solid line in Fig. 29a. The phase shifts of this P-wave potential are practically the same as those shown by the solid line in Fig. 9a.

To study transitions with $\Delta T=0$ it is necessary to use the repulsive P-wave potential from the p^3H system given in Table IX. Here it is not possible at all to correctly reproduce

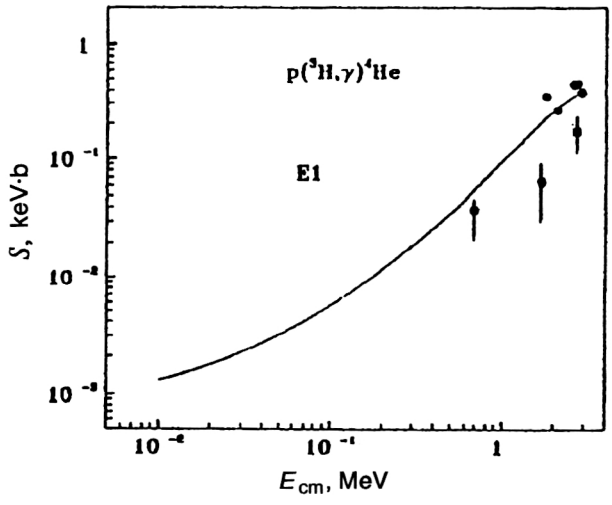

FIG. 30. Astrophysical S factor for p^3H capture. The solid line was calculated for the potentials of Tables IV, VIII, and IX. The points, triangles, squares, and circles are the experimental data from Refs. 86–91.

even the shape of the experimental cross sections, as shown by the dot–dash line in Fig. 29a.

In Fig. 29b the dashed line shows the calculated results for the reaction ^{4}He$(\gamma,n)^3$He with $\Delta T=1$ for the P-wave interaction of Table IV together with the experimental data of Refs. 89 (points), 90 (triangles), and 91 (circles). Here the earlier measurements of the cross sections[92] lie considerably higher than the later ones.[89,90] If the depth in the P wave is decreased slightly to 11 MeV while keeping the geometry unchanged, it is possible to describe the data of Refs. 89 and 90. This cross section is shown by the solid line in Fig. 29b. The phase shifts of this P-wave potential are shown by the dotted line in Fig. 9a and agree with the results of the phase-shift analysis from Ref. 44.

The existing calculations of the cross sections for these photoreactions using various models and approaches (see, for example, Refs. 86–91) in general lead to agreement with the available experimental data. However, the experimental uncertainties are so large that it is difficult to favor any particular set of results. In this situation the nonuniqueness of the phase-shift analyses makes it possible to slightly change the potential parameters and obtain results which agree with certain experimental data on photodisintegration.

In Fig. 30 we show the astrophysical S factor at low energies obtained using the P-wave interaction of depth 15 MeV, which describes the photodisintegration process. The experimental data are from Refs. 86–89. We see that, in spite of the large experimental errors, on the whole the measured cross sections[86–89] are reproduced even at low energies of 0.7–3 MeV. Linear extrapolation of the S factor to zero energy gives a value of about $1.3(6)\times10^{-3}$ keV·b.

CONCLUSION

On the basis of these results, it can be stated that the calculations of the elastic and inelastic Coulomb form factors of lithium nuclei using two-cluster models with potentials containing forbidden states allow a reasonable description of the experimental results even at relatively large momentum transfers. In contrast to the RGM calculations,[34–36] in all cases the form factor contains a second maximum which is slightly lower than the experimental data. It is possible to reproduce the $E2$ and $M1$ electromagnetic transition probabilities, the magnetic, quadrupole, and octupole moments, and the magnetic and charge radii. The potential parameters were at first fixed using the phase shifts of cluster elastic scattering, and then changed slightly in the calculation of the form factors only for the D_3 wave in ^{6}Li, which allowed good reproduction of the behavior of the first maximum in the form factor.

The cluster potential model for interactions containing forbidden states allows the correct description of not only the static electromagnetic characteristics of lithium nuclei, but also the total cross sections for photoprocesses in the entire energy range studied. The S factors at astrophysical energies are also described. It can therefore be assumed that the large clusterization probability of lithium nuclei in the ^{4}He^{2}H and ^{4}He^{3}H channels allows the simple one-channel cluster model to be used quite successfully. The same sets of potentials can be used to describe different nuclear characteristics. It is not necessary to introduce any distortion of the cluster characteristics to obtain agreement with experiment. The assumption that on the whole a given cluster in the nucleus can be associated with the properties of the corresponding free particle is completely justified. This is consistent also with the RGM results,[36,92] where distortions lead only to insignificant changes in the characteristics of ^{6}Li and ^{7}Li nuclei. The only exception is the ^{3}He^{3}H capture cross section, where there are some experimental ambiguities in the cross sections, and the phase shifts and ground-state energies cannot be made to agree.

The use of the one-channel cluster potential model with forbidden states and separation on the basis of Young schemes makes it possible on the whole to reproduce the available experimental data on the total cross sections for photodisintegration and radiative capture in the N^{2}H system at low energies using a potential which on the whole is consistent with the pure phase shifts, the scattering phase shifts, and bound-state characteristics. It can also be used to obtain specific results for the ^{2}H^{3}He system.

In general, the cluster potential model reproduces the shape of the cross sections for ^{4}He photodisintegration using $E1$ transitions with $\Delta T=1$ for reactions in the p^3H and p^3He channels. The calculated cross sections lie within the range of uncertainty of the various experimental results. By varying the P-wave interaction depth by 10–20%, it is possible to slightly improve the agreement between the calculations and some of the experimental data on the cross sections for photoprocesses. The phase shifts of the P-wave potentials modified in this way lie within the range of experimental uncertainties of the various phase-shift analyses. The ground-state potential is consistent with the bound-state characteristics and pure phase shifts.

The cluster model with separation on the basis of Young schemes allows description of some of the experimental data on the total cross sections for photodisintegration and radiative capture in the ^{2}H^{2}H channel at low energies. The astrophysical S factor is in complete agreement with the results of

other calculations at energies which are not too low. It proves possible to eliminate the uncertainties in the choice of the ground-state S-wave potential of the nucleus and to make its parameters consistent with pure phase shifts. This improves both the form and the structure of the singlet D-wave interaction, allowing the phase shifts and cross sections for photoprocesses to be reproduced simultaneously.

[1] V. G. Neudatchin *et al.*, Lett. Nuovo Cimento **5**, 234 (1972); Phys. Lett. B **34**, 581 (1971).
[2] V. G. Neudachin and Yu. F. Smirnov, in *Current Problems in Optics and Atomic Physics* [in Russian] (Kiev State University Press, Kiev, 1974), p. 224; Fiz. Élem. Chastits At. Yadra **10**, 1236 (1979) [Sov. J. Part. Nucl. **10**, 492 (1979)].
[3] S. B. Dubovichenko and A. V. Dzhazairov-Kakhramanov, Yad. Fiz. **56**, No. 2, 87 (1993) [Phys. At. Nucl. **56**, 195 (1993)]; Yad. Fiz. **57**, 784 (1994) [Phys. At. Nucl. **57**, 733 (1994)].
[4] D. R. Lehman *et al.*, Phys. Lett. B **59**, 327 (1975); Phys. Rev. C **25**, 2743, 3146 (1982).
[5] V. G. Neudachin and Yu. F. Smirnov, *Nucleon Associations in Light Nuclei* [in Russian] (Nauka, Moscow, 1969).
[6] V. G. Neudachin *et al.*, Phys. Rev. C **45**, 1512 (1992); Fiz. Élem. Chastits At. Yadra **23**, 479 (1992) [Sov. J. Part. Nucl. **23**, 210 (1992)].
[7] V. G. Neudachin *et al.*, Yad. Fiz. **52**, 738, 402 (1990) [Sov. J. Nucl. Phys. **52**, 473, 258 (1990)]; V. Iskra *et al.*, Ukr. Fiz. Zh. **32**, 1141 (1988) [in Russian]; Yad. Fiz. **48**, 1674 (1988) [Sov. J. Nucl. Phys. **48**, 1003 (1988)]; S. B. Dubovichenko *et al.*, Izv. Akad. Nauk SSSR, Ser. Fiz. **54**, 911 (1990) [Bull. Acad. Sci. USSR, Phys. Ser.].
[8] S. B. Dubovichenko and A. V. Dzhazairov-Kakhramanov, Yad. Fiz. **51**, 1541 (1990) [Sov. J. Nucl. Phys. **51**, 971 (1990)]; Yad. Fiz. **56**, No. 4, 45 (1993) [Phys. At. Nucl. **56**, 447 (1993)].
[9] S. B. Dubovichenko and A. V. Dzhazairov-Kakhramanov, Yad. Fiz. **55**, 2918 (1992) [Sov. J. Nucl. Phys. **55**, 1632 (1992)]; S. B. Dubovichenko, A. V. Dzhazairov-Kakhramanov, and A. A. Sakharuk, Yad. Fiz. **56**, No. 8, 90 (1993) [Phys. At. Nucl. **56**, 1044 (1993)]; S. B. Dubovichenko, Yad. Fiz. **60**, 195 (1997) [Phys. At. Nucl. **60**, 195 (1997)].
[10] S. B. Dubovichenko and A. V. Dzhazairov-Kakhramanov, Yad. Fiz. **58**, 635, 852 (1995) [Phys. At. Nucl. **58**, 579, 788 (1995)].
[11] T. Tombrello *et al.*, Phys. Rev. **131**, 2578 (1963).
[12] T. Mertelmeir *et al.*, Nucl. Phys. A **459**, 387 (1986).
[13] B. Buck *et al.*, J. Phys. G **11**, L11 (1985).
[14] J. C. Bergstrom, Nucl. Phys. A **341**, 13 (1980).
[15] V. I. Kukulin *et al.*, Nucl. Phys. A **417**, 128 (1984); **453**, 365 (1986); **517**, 221 (1990).
[16] E. Itzykson, Rev. Mod. Phys. **38**, 95 (1966).
[17] D. Baye *et al.*, J. Phys. G **7**, 1073 (1981); D. Tompson *et al.*, Phys. Rev. **159**, 806 (1967).
[18] P. Schmelzbach *et al.*, Nucl. Phys. A **184**, 193 (1972); L. McIntair *et al.*, Nucl. Phys. A **91**, 382 (1967); M. Bruno *et al.*, Nuovo Cimento A **68**, 35 (1982); B. Jenny *et al.*, Nucl. Phys. A **397**, 61 (1983); P. Darriulat *et al.*, Nucl. Phys. A **94**, 653 (1967); L. Keller *et al.*, Nucl. Phys. A **156**, 465 (1970); I. Ya. Barit *et al.*, Preprint No. P-0513, Nuclear Research Institute, Moscow (1987) [in Russian].
[19] A. Bernard *et al.*, Nucl. Phys. **50**, 629 (1964); R. Spiger *et al.*, Phys. Rev. **163**, 964 (1967).
[20] M. Ivanovich *et al.*, Nucl. Phys. A **110**, 441 (1968).
[21] J. Vlastou *et al.*, Nucl. Phys. A **292**, 29 (1977); R. Batten *et al.*, Nucl. Phys. A **151**, 56 (1970).
[22] D. Tompson *et al.*, Nucl. Phys. A **106**, 591 (1968).
[23] F. Ajzenberg-Selove, Nucl. Phys. A **320**, 1 (1979); S. Fiarman *et al.*, Nucl. Phys. A **206**, 1 (1973).
[24] A. Bacher *et al.*, Nucl. Phys. A **119**, 481 (1968).
[25] D. Beck *et al.*, Phys. Rev. C **30**, 1403 (1984); G. Simon *et al.*, Nucl. Phys. A **365**, 285 (1981); S. Klasfeld *et al.*, Nucl. Phys. A **456**, 373 (1986); B. Borie *et al.*, Nucl. Phys. A **275**, 246 (1977); Phys. Rev. A **18**, 324 (1978); P. Dunn *et al.*, Phys. Rev. C **27**, 71 (1983); I. Sick *et al.*, Phys. Lett. B **116**, 212 (1982).
[26] G. Van Niftric *et al.*, Nucl. Phys. A **174**, 173 (1971); O. Hausser *et al.*, Nucl. Phys. A **212**, 613 (1973); S. Green *et al.*, Phys. Rev. A **4**, 251 (1971); D. Sundholm *et al.*, Chem. Phys. Lett. **112**, 1 (1984); W. Vermeer *et al.*, Aust. J. Phys. **37**, 273 (1984); Phys. Lett. B **138**, 365 (1984); A. Weller *et al.*, Phys. Rev. Lett. **55**, 480 (1985); A. Bamberger *et al.*, Nucl. Phys. **194**, 193 (1972); H. De Vries *et al.*, At. Data Nucl. Data Tables **36**, 495 (1987).
[27] D. Platner, in *Proceedings of the European Conf. on Few-Body Problems in Nuclear and Particle Physics*, Sesimbra., 1980, p. 31; M. Bornard *et al.*, Nucl. Phys. A **294**, 492 (1978); T. Lim, Phys. Rev. C **14**, 1243 (1976).
[28] K. Wildermuth and Y. C. Tang, *A Unified Theory of the Nucleus* (Academic Press, New York, 1977) [Russ. transl., Mir, Moscow, 1980].
[29] É. V. Lan'ko *et al.*, *Electromagnetic Transition Probabilities of Nuclei* [in Russian] (Nauka, Leningrad, 1972).
[30] K. Rao *et al.*, Phys. Scr. **24**, 925 (1981); Q. Liu *et al.*, Z. Phys. **303**, 253 (1981); M. Bouten *et al.*, J. Phys. G **8**, 1641 (1982).
[31] B. Buck *et al.*, J. Phys. G **14**, L211 (1988).
[32] P. Roos *et al.*, Nucl. Phys. A **257**, 317 (1976); J. Watson *et al.*, Nucl. Phys. A **172**, 513 (1971); J. Alder *et al.*, Phys. Rev. C **6**, 1 (1972).
[33] T. Janssens *et al.*, Phys. Rev. **142**, 922 (1966).
[34] A. Kruppa *et al.*, Phys. Lett. B **179**, 317 (1986); Phys. Rev. C **36**, 327 (1987); V. Sharma *et al.*, J. Phys. G **10**, 1703 (1984); T. Kajino *et al.*, Nucl. Phys. A **413**, 323 (1984); **414**, 185 (1984); T. Kaneko *et al.*, Phys. Rev. C **43**, 771 (1986).
[35] M. Unkelbach and H. Hofman, Phys. Lett. B **261**, 211 (1991); Few-Body Syst. **11**, 143 (1991).
[36] H. Kanada *et al.*, Nucl. Phys. A **389**, 285 (1982); Prog. Theor. Phys. **72**, 369 (1984).
[37] Il-Tong Cheon, Phys. Lett. B **30**, 81 (1969); **35**, 276 (1971); Phys. Rev. C **3**, 1023 (1971).
[38] J. Bergstrom, Nucl. Phys. A **262**, 196 (1976); **327**, 458 (1979); Phys. Rev. C **25**, 1156 (1982).
[39] H. Walliser and T. Fliesbach, Phys. Rev. C **31**, 2242 (1985).
[40] J. Lichtenstadt *et al.*, Phys. Lett. B **219**, 394 (1989); **244**, 173 (1990); J. McGarthy *et al.*, Phys. Rev. C **15**, 1396 (1977); R. G. Arnold *et al.*, Phys. Rev. Lett. **40**, 1429 (1978).
[41] V. I. Kukulin *et al.*, Preprint R-0685, Nuclear Physics Institute, USSR Academy of Sciences (1990) [in Russian]; Izv. Akad. Nauk SSSR, Ser. Fiz. **53**, 121 (1989) [Bull. Acad. Sci. USSR, Phys. Ser.]; Izv. Akad. Nauk Kazakh SSR, Ser. Fiz.-Mat. No. 2, 44 (1988) [in Russian]; J. Phys. G **58**, 777 (1989); R. A. Eramzhyan *et al.*, Phys. Lett. B **228**, 1 (1989).
[42] H. Berg *et al.*, Nucl. Phys. A **334**, 21 (1980); R. Kavanagh *et al.*, Phys. Rev. **143**, 143 (1966).
[43] D. McSherry *et al.*, Phys. Rev. C **1**, 888 (1970); G. Szaloky *et al.*, Nucl. Phys. A **303**, 57 (1978); L. Morrow *et al.*, Nucl. Phys. A **126**, 225 (1969).
[44] T. Tombrello *et al.*, Phys. Rev. **138**, B40 (1965).
[45] L. Drigo *et al.*, Nuovo Cimento B **51**, 419 (1967).
[46] J. Morales *et al.*, Phys. Rev. C **11**, 1905 (1975); B. Mudroch *et al.*, Phys. Rev. C **29**, 2001 (1984).
[47] T. Tombrello, Phys. Rev. **143**, 772 (1966).
[48] P. Shen *et al.*, Phys. Rev. C **33**, 1214 (1986); M. LeMere *et al.*, Phys. Rev. C **12**, 1140 (1975).
[49] P. Schmelzbach *et al.*, Nucl. Phys. A **197**, 237 (1972); J. Arviex, Nucl. Phys. A **102**, 513 (1967); W. van Oers, Nucl. Phys. A **92**, 561 (1967); J. Chauvin *et al.*, Nucl. Phys. A **247**, 347 (1975); J. Sloan, Nucl. Phys. A **168**, 211 (1971); E. Huttel *et al.*, Nucl. Phys. A **406**, 443 (1983).
[50] D. Kocher *et al.*, Nucl. Phys. A **132**, 455 (1969).
[51] I. Sick *et al.*, Phys. Rev. Lett. **45**, 871 (1980); C. Atti *et al.*, *Lecture Notes in Physics*, Vol. 137 (1981), p. 115.
[52] B. Jenny, Nucl. Phys. A **337**, 77 (1980).
[53] H. Kanada *et al.*, Nucl. Phys. A **457**, 93 (1986); **504**, 529 (1989); P. Shen *et al.*, Phys. Rev. C **31**, 2001 (1985).
[54] J. Brolley *et al.*, Phys. Rev. **117**, 1307 (1960); T. King *et al.*, Nucl. Phys. A **183**, 657 (1972).
[55] P. Lien, Nucl. Phys. A **178**, 375 (1972).
[56] H. Kanada *et al.*, Phys. Rev. C **34**, 22 (1986).
[57] R. Frank *et al.*, Phys. Rev. **99**, 1406 (1953); R. Darves-Blane, Nucl. Phys. A **191**, 353 (1972); J. Detch *et al.*, Phys. Rev. C **4**, 52 (1971); C. Werntz *et al.*, Nucl. Phys. A **121**, 38 (1968); W. Meyerhof *et al.*, Nucl. Phys. **74**, 533 (1965); I. Ya. Barit and V. A. Sergeev, Yad. Fiz. **13**, 1230 (1971) [Sov. J. Nucl. Phys. **13**, 708 (1971)].
[58] R. Hardekopf *et al.*, Nucl. Phys. A **191**, 481 (1972); R. Kankovsky *et al.*, Nucl. Phys. A **263**, 29 (1976).
[59] K. Langanke, Nucl. Phys. A **457**, 351 (1986).
[60] Q. Liu *et al.*, Phys. Rev. C **23**, 645 (1981); L. Walliser *et al.*, Nucl. Phys. A **419**, 133 (1984); Phys. Rev. C **28**, 57 (1983).
[61] T. Kajino, Nucl. Phys. A **460**, 559 (1986).
[62] N. Burkova *et al.*, Phys. Lett. B **248**, 15 (1990); V. P. Denisov and I. Ya.

Chubukov, Yad. Fiz. **35**, 11 (1982) [Sov. J. Nucl. Phys. **35**, 6 (1982)].
[63]P. Parker *et al.*, Phys. Rev. **131**, 2582 (1963); K. Nagatani *et al.*, Nucl. Phys. A **128**, 325 (1969); J. Osborn *et al.*, Phys. Rev. Lett. **42**, 1664 (1982); Nucl. Phys. A **419**, 115 (1984); R. Robertson *et al.*, Phys. Rev. C **27**, 11 (1983); H. Krawinkel *et al.*, Z. Phys. **304**, 307 (1982).
[64]G. Griffiths *et al.*, Can. J. Phys. **39**, 1397 (1961).
[65]W. Fowler *et al.*, Annu. Rev. Astron. Astrophys. **13**, 69 (1975).
[66]T. Aleksander *et al.*, Nucl. Phys. A **427**, 526 (1984).
[67]B. Buck *et al.*, Nucl. Phys. A **275**, 246 (1976); in *Proceedings of the Fourth Intern. Conf. on Cluster Aspects of Nuclear Structure and Nuclear Reactions*, Chester, 1984.
[68]R. Robertson *et al.*, Phys. Lett. B **47**, 1867 (1981).
[69]H. Taneichi *et al.*, Nucl. Phys. A **448**, 315 (1986); D. Skopik *et al.*, Phys. Rev. C **14**, 789 (1976).
[70]M. A. Zhusupov *et al.*, Izv. Akad. Nauk Kazakh SSR, Ser. Fiz.-Mat. **2**, 30 (1991) [in Russian].
[71]A. Young *et al.*, Phys. Rev. Lett. **25**, 1764 (1970); S. Blatt *et al.*, Phys. Rev. **176**, 1147 (1968).
[72]F. Nusslin *et al.*, Z. Naturforsch. A **21**, 1195 (1966).
[73]A. Murakami *et al.*, Nuovo Cimento B **60**, 604 (1968); J. Phys. Soc. Jpn. **28**, 191 (1970); E. Bazhanov *et al.*, Nucl. Phys. A **65**, 191 (1965); N. Sherman *et al.*, Phys. Rev. **169**, 771 (1968); Phys. Rev. Lett. **17**, 31 (1966).
[74]A. Mondragon *et al.*, Phys. Rev. C **41**, 1975 (1990).
[75]S. B. Dubovichenko, Yad. Fiz. **58**, 1253 (1995) [Phys. At. Nucl. **58**, 1174 (1995)].
[76]V. N. Fetisov *et al.*, Nucl. Phys. **71**, 305 (1965); J. R. Stewart *et al.*, Phys. Rev. **138**, B372 (1965); S. K. Kundu *et al.*, Nucl. Phys. A **171**, 384 (1971); B. L. Berman *et al.*, Phys. Rev. **133**, B117 (1964).
[77]D. D. Faul *et al.*, Phys. Rev. C **24**, 849 (1981); D. M. Skopik *et al.*, Phys. Rev. C **24**, 1791 (1981).
[78]G. M. Griffiths *et al.*, Can. J. Phys. **40**, 402 (1962).
[79]H. Weller and D. Lehman, Annu. Rev. Nucl. Part. Sci. **38**, 563 (1988); G. Bluge *et al.*, Phys. Rev. C **36**, 21 (1987); H. Assenbaum and K. Langanke, Phys. Rev. C **36**, 17 (1987); B. Wachter *et al.*, Phys. Lett. B **200**, 246 (1988).
[80]S. B. Dubovichenko, Yad. Fiz. **58**, 1973 (1995) [Phys. At. Nucl. **58**, 1866 (1995)].
[81]R. Zurmuhle *et al.*, Phys. Rev. **132**, 751 (1963); W. Meyerhof *et al.*, Nucl. Phys. A **131**, 489 (1969); F. Wilkinson and F. Cecil, Phys. Rev. C **31**, 2036 (1985).
[82]D. Skopik and W. Dodge, Phys. Rev. C **6**, 43 (1972).
[83]Yu. M. Arkatov *et al.*, Ukr. Fiz. Zh. **23**, 918 (1978) [in Russian].
[84]S. B. Dubovichenko, Yad. Fiz. **58**, 1377 (1995) [Phys. At. Nucl. **58**, 1295 (1995)].
[85]B. Gibson, Nucl. Phys. A **353**, 85 (1981).
[86]W. Meyerhof *et al.*, Nucl. Phys. A **148**, 211 (1970); Yu. Arkatov *et al.*, Yad. Fiz. **10**, 1123 (1969) [Sov. J. Nucl. Phys. **10**, 639 (1970)]; **12**, 227 (1970); [**12**, 123 (1971)]; **21**, 925 (1975) [**12**, 475 (1975)].
[87]D. Gemmel *et al.*, Nucl. Phys. **33**, 102 (1962); A. Gorbunov, Phys. Lett. B **27**, 436 (1968).
[88]R. Bernabei *et al.*, Phys. Rev. C **38**, 1990 (1988).
[89]F. Balestra *et al.*, Nuovo Cimento A **38**, 145 (1977).
[90]J. Calarco *et al.*, Phys. Rev. C **27**, 1866 (1983); B. Berman *et al.*, Phys. Rev. C **22**, 2273 (1980).
[91]J. Irish *et al.*, Can. J. Phys. **53**, 802 (1975).
[92]J. Susila *et al.*, Acta Phys. Pol. B **12**, 799 (1981); M. Mihailovic *et al.*, Nucl. Phys. A **363**, 377 (1981); R. Krivec *et al.*, J. Phys. G **8**, 821 (1982); H. Kanada *et al.*, Nucl. Phys. A **380**, 87 (1982).

Translated by Patricia A. Millard